Defining the Immune Responses for SARS-CoV-2-Human Macrophage Interactions

Mai M. Abdelmoaty[1,2], Pravin Yeapuri[1], Jatin Machhi[3], Katherine E. Olson[3], Farah Shahjin[3], You Zhou[4], Liang Jingjing[3], Kabita Pandey[3], Arpan Acharya[3], Siddappa N. Byrareddy[3], R. Lee Mosley[3] and Howard E. Gendelman[3*]

[1]Department of Pharmaceutical Sciences, College of Pharmacy, University of Nebraska Medical Center, NE 68198, USA

[2]Therapeutic Chemistry Department, Pharmaceutical and Drug Industries Research Division, National Research Centre, Giza, Egypt

[3]Department of Pharmacology and Experimental Neuroscience, College of Medicine, University of Nebraska Medical Center, NE 68198, USA

[4]Center for Biotechnology, University of Nebraska-Lincoln, Lincoln, NE, USA

***Corresponding author:** Howard E. Gendelman, Department of Pharmacology and Experimental Neuroscience, University of Nebraska Medical Center, Omaha, NE 68198-5800; phone 402-559-8920; fax 402-559-3744; email hegendel@unmc.edu

Abstract

Host innate immune response follows severe acute respiratory syndrome coronavirus 2 (SARS-CoV-2) infection, and it is the driver of the acute respiratory distress syndrome (ARDS) amongst other inflammatory end-organ morbidities. Such life-threatening coronavirus disease 2019 (COVID-19) is heralded by virus-induced activation of mononuclear phagocytes (MPs; monocytes, macrophages, and dendritic cells). MPs play substantial roles in aberrant immune secretory activities affecting profound systemic inflammation and end organ malfunctions. All follow an abortive viral infection. To elucidate SARS-CoV-2-MP interactions we investigated transcriptomic and proteomic profiles of human monocyte-derived macrophages. While expression of the SARS-CoV-2 receptor, the angiotensin-converting enzyme 2, paralleled monocyte-macrophage differentiation it failed to affect productive viral infection. In contrast, simple macrophage viral exposure led to robust pro-inflammatory cytokine and chemokine expression but attenuated type I interferon (IFN) activity. Both paralleled dysregulation of innate immune signaling pathways specifically those linked to IFN. We conclude that the SARS-CoV-2-infected host mounts a robust innate immune response characterized by a pro-inflammatory storm heralding consequent end-organ tissue damage.

Keywords: macrophages, SARS-CoV-2, cytokine storm, interferon, end-organ disease, inflammation, transcriptomics, proteomics

Introduction

Severe acute respiratory syndrome coronavirus 2 (SARS-CoV-2), the causative agent of coronavirus disease 2019 (COVID-19), is an enveloped positive-stranded RNA virus belonging to the *Coronaviridae* family, *Betacoronaviruses* genus (Lu et al., 2020). COVID-19 has posed an unprecedented global threat to public health and in March of 2020, it was declared a pandemic by the World Health Organization (WHO) (World Health Organization, 2020). COVID-19 ranges from asymptomatic infection to mild pneumonia and, in its most severe form, progression to acute respiratory distress syndrome (ARDS). Such pulmonary compromise is associated with dyspnea and hypoxia that can progress to severely compromised lung dysfunction and multiorgan system failure and death (Gavriatopoulou et al., 2020). Disease mortality is linked to cytokine storm syndrome (CSS), heralded by innate immune activation with secretion of excessive pro-inflammatory cytokines (Ruan et al., 2020). Indeed, nearly 15% of reported COVID-19 disease cases progress to ARDS defined by widespread inflammatory-associated lung tissue damage and multiorgan failure (Guan et al., 2020) involving heart, liver, gastrointestinal tract, kidney, and brain (Salamanna et al., 2020). Viral persistence in the face of such end-organ disease is linked to cell expression of angiotensin-converting enzyme 2 (ACE2), the molecule that SARS-CoV-2 utilizes for receptor-mediated cell entry (Wan et al., 2020).

Mononuclear phagocytes (MPs; monocytes, macrophages, and dendritic cells) are the governors of innate immunity serving to contain microbial infection (Lugo-Villarino et al., 2019). Immediately following viral exposure, the process of intracellular microbial removal is initiated through recognition of viral pathogen-associated molecular patterns (PAMPs) by pattern recognition receptors (PRRs). This includes, but is not limited to, cytosolic retinoic acid-inducible

67 gene I (RIG-I)-like receptors (RLRs) and extracellular and endosomal toll-like receptors (TLRs).
68 During the initiation of virus-cell interactions, secretion of pro-inflammatory cytokines and
69 chemokines initiate intracellular killing, antigen presentation, and mobilization of adaptive
70 immunity. Factors that are engaged include, but are not limited to, interleukin-6 (IL-6), IL-1, tumor
71 necrosis factor-alpha (TNF-α), and C-X-C motif chemokine ligand 10 (CXCL10) (Nikitina et al.,
72 2018). Type I interferon (IFN) α and β responses occur in tandem to control both viral replication
73 and dissemination (Swiecki and Colonna, 2011). During infection with SARS-CoV-2, CSS
74 contributes to COVID-19-associated multiorgan failure (Huang et al., 2020; Xiong et al., 2020).
75 In particular, infiltrating inflammatory MPs in lungs, heart, kidney, spleen, and lymph nodes are
76 seen in post-mortem tissues of COVID-19-infected patients (Diao et al., 2021; Feng et al., 2020;
77 Merad and Martin, 2020; Xu et al., 2020). Despite the critical role of MPs to clear the infection,
78 these same cells underlie the pathobiology of COVID-19.
79
80 Mounting evidence confirms abortive MP infection by SARS-CoV-2 (Yang et al., 2020; Zheng et
81 al., 2021). Nonetheless, such viral cell engagements are sufficient to induce activation and pro-
82 inflammatory cytokine secretory responses. The nature of virus-MP interactions and their role in
83 persistent viral infection and associated tissue pathologies remains enigmatic. To such ends, we
84 pursued transcriptomic and proteomic analyses of immune cells following virus infection to
85 identify modulations of host immune responses. We employed MPs to assess immune responses
86 following SARS-CoV-2 cell engagements for cell activation using human immune response arrays
87 and mass spectrometry-based label-free proteomic quantification methods. These techniques serve
88 to define virus-induced innate immune responses linked to antiviral immunity. Based on these
89 tests, we have uncovered the dysregulation of a spectrum of viral-induced responses related to IFN

90 signaling pathways, complement activation, and linked adaptive immune responses. All provide
91 unique insight into how the inflammatory response occurs as a consequence of SARS-CoV-2
92 infection. Virion persistence for up to 14 days after viral exposure despite abortive infection
93 underlies the persistence of immune activation. Most importantly, the data provides a signature
94 for virus-induced disease pathobiology, including COVID-19-associated CSS and multiorgan
95 dysfunction. All affect the most severe disease morbidities and mortalities seen as a consequence
96 of viral exposure, transmission, and dissemination.
97

98 **Materials and methods**

99 **Isolation and cultivation of human monocytes**

100 Human monocytes were obtained by leukapheresis from hepatitis B and HIV-1/2 seronegative
101 donors and purified by counter-current centrifugal elutriation (Faradji et al., 1994). Monocytes
102 were seeded in 6-well plates ($3x10^6$ cells/well) in Dulbecco's Modified Eagle's Media (DMEM)
103 containing 4.5 g/l glucose, L-glutamine, and sodium pyruvate, and supplemented with 10% heat-
104 inactivated human serum, 50 µg/ml gentamicin, 10 µg/ml ciprofloxacin, and 1000 U/ml human
105 macrophage colony-stimulating factor (M-CSF) to facilitate differentiation of monocytes into
106 monocyte-derived macrophages (MDMs). Cells were incubated at 37°C with 5% CO_2, and the
107 culture medium was half-exchanged with fresh medium every other day (Gendelman et al., 1992).
108

109 **Flow cytometry assays**

110 Human monocytes were evaluated by flow cytometry for levels of SARS-CoV-2 cell entry
111 receptor ACE2 and monocyte-macrophage phenotypic surface markers, CD14 and CD16, during
112 macrophage differentiation with or without captopril (Sigma-Aldrich, C4042). Captopril was

113 added to the culture medium to increase ACE2 cell expression. On days 0, 1, 3, 5, and 7 during
114 differentiation, monocytes-macrophages were stained with fluorescently-conjugated antibodies to
115 detect human ACE2 (APC, LSBio, LS-C275129, polyclonal), CD14 (Alexa Fluor 488,
116 eBioscience, clone 61D3), and CD16 (PE, eBioscience, eBioCB16, clone CB16), and with isotype-
117 matched antibodies serving as negative controls. Stained cells were examined with an LSR II flow
118 cytometer (BD Biosciences) and analyzed using BD FACSDiva software.
119
120 **SARS-CoV-2 infection**
121 Experiments involving SARS-CoV-2 were performed in the University of Nebraska Medical
122 Center (UNMC) biosafety level 3 (BSL-3) core facility and approved by UNMC Institutional
123 Biosafety Committee (IBC) (protocol number 20-05-027-BL3). The SARS-CoV-2 strain used in
124 this study was isolate USA-WI1/2020 (BEI, NR-52384). The virus was passaged on Vero.STAT1
125 knockout (KO) cells (ATCC, CCL-81-VHG) and titer was determined by plaque assay in Vero E6
126 cells (ATCC, CRL-1586) (Mendoza et al., 2020). On day 5 following cell cultivation, MDMs were
127 exposed to the WI1/2020 viral strain at a multiplicity of infection (MOI) of 0.01. Exposure was
128 maintained with or without captopril, and the virus-cell mixtures incubated at 37°C in 5% CO_2
129 with shaking at 15 minute intervals for 1 hour. This was followed by incubation with the virus for
130 an additional 3 hours. At the termination of viral cell incubation, the virus inoculum was removed,
131 and cells were washed 3 times with phosphate-buffered saline (PBS). Mock-challenged cells were
132 treated with a culture medium alone. Culture supernatants were collected at defined time points
133 then used for viral quantitative reverse transcription-polymerase chain reaction (RT-qPCR) and
134 type I IFN activity assays. Vero.STAT1 KO cells were maintained for study based on their high
135 susceptibility to virus infection due to lack of Signal Transducer and Activator of Transcription 1

136 (STAT1) protein required for cellular antiviral responses (Durbin et al., 1996). Thus, the SARS-
137 CoV-2 replication kinetics in MDMs were compared against viral infection in Vero.STAT1 KO
138 cells that were monitored over 5 days post-viral exposure.
139
140 **RT-qPCR assay**
141 Culture supernatants were collected on days 1, 3, 5, 7, and 10 following viral exposure. Viral
142 RNA was extracted using QIAamp Viral RNA Mini Kit (Qiagen, 52906). SARS-CoV-2 genome
143 equivalents were quantified in culture supernatant by RT-qPCR using 2019-nCoV CDC probe and
144 Primer Kit for SARS-CoV-2 (Biosearch Technologies, KIT-nCoV-PP1-1000). Forward primer: 5'
145 GACCCCAAAATCAGCGAAAT 3', Reverse primer: 5' TCTGGTTACTGCCAGTTGAATCTG
146 3', and Probe: 5' FAM-ACCCCGCATTACGTTTGGTGGACC-BHQ-1 3'. RT-qPCR was
147 performed using Taqman Fast Virus 1-step Master Mix (Thermo Fisher Scientific, 4444434) in
148 StepOne Plus real-time PCR thermocycler (Applied Biosystems) using the following cycling
149 conditions: 50°C for 10 minutes, 95°C for 3 minutes, and 40 cycles of 95°C for 15 seconds,
150 followed by 60°C for 1 minute. The SARS-CoV-2 genome equivalent copies were calculated using
151 control RNA from heat-inactivated SARS-CoV-2 USA-WA1/2020 (BEI, NR-52347).
152
153 **Transmission electron microscopy (TEM)**
154 For negative staining analysis of viral particles used for cell infection experiment, purified SARS-
155 CoV-2 viruses were de-activated and fixed in 2% glutaraldehyde and 2% paraformaldehyde (PFA)
156 in 0.1 M Sorenson's phosphate buffer for 1 hour at room temperature. Briefly, for negative
157 staining, a drop of the virus sample in a fixative solution was placed onto a formvar and carbon-
158 coated grid for 30-40 seconds. After removing excess sample solution with filter paper, the grid

159 was placed with sample side down on a drop of 1% phosphotungstic acid (PTA) in water, stained
160 for 30 seconds, then excess PTA solution was blotted with filter paper. Stained samples were
161 examined and imaged using a Hitachi H7500 TEM (Hitachi High-Tech GLOBAL) and a bottom-
162 mount AMT camera (AMT Imaging). For ultrastructural analysis, mock and SARS-CoV-2-
163 challenged MDMs sampled at 1, 3, and 5 days post-viral inoculation were washed 2 times with
164 PBS and fixed in a solution of 2% glutaraldehyde and 2% PFA in 0.1 M Sorenson's phosphate
165 buffer for 24 hours at 4°C which have been washed 3 times with PBS to clear excess fixative
166 solution. TEM analysis was performed as previously described (Mukadam et al., 2020) in samples
167 post-fixed in a 1% aqueous solution of osmium tetroxide for 30 minutes that were dehydrated in
168 50, 70, 90, 95, and 100% graded ethanol. Spurr's resin was used as embedding medium after
169 solvent transition with ethanol and Spurr's resin (50:50 ethanol:resin, followed by twice immersion
170 in 100% Spurr's resin for 2-3 hours for each solution), and embedded samples were cured at 60 -
171 65°C for 24 hours. Ultrathin sections (100 nm) were cut with Leica UC7 ultramicrotome, placed
172 on 200-mesh copper grids, followed by staining with 2% uranyl acetate and Reynold's lead citrate,
173 and examined with a Hitachi H7500 TEM at 80 kV. Images were acquired digitally with an AMT
174 digital imaging system.
175
176 **Transcriptomic analyses**
177 SARS-CoV-2-challenged MDMs were collected on days 1, 3, and 5 post-viral exposure. Total
178 RNA was isolated using RNeasy Mini Kit (Qiagen, 74104), and cDNA was generated utilizing
179 RevertAid First Strand cDNA synthesis kit (Thermo Fisher Scientific, K1622) followed by
180 amplification and quantification using RT^2 Profiler Human Innate and Adaptive Immune Response
181 96-well Array (Qiagen, 330231) with RT^2 SYBR Green ROX qPCR Mastermix (Qiagen, 330523).

182 The qPCR cycling conditions were 95°C for 10 minutes for 1 cycle, followed by 40 cycles of 95°C
183 for 15 seconds and 60°C for 1 minute using Eppendorf Mastercycler ep realplex 2S. Fold changes
184 were determined via Qiagen's RT^2 Profiler analysis software (version 3.5). Ingenuity Pathway
185 Analysis (IPA) (Qiagen) was used to identify the pathways and networks affected post-viral
186 exposure. Functional and pathway enrichment analyses of screened genes in SARS-CoV-2-
187 challenged MDMs were compared to mock-challenged MDMs at different time intervals following
188 viral exposure. Gene ontology (GO) annotation was conducted using the GO Resource database
189 (http://geneontology.org). The Kyoto Encyclopedia of Genes and Genomes (KEGG) pathway
190 enrichment analysis was conducted utilizing DAVID (http://david.abcc.ncfcrf.gov/) (Huang da et
191 al., 2009), an online tool providing a comprehensive set of functional annotations for
192 understanding biological meaning in large list of genes. The Reactome gene set enrichment
193 analysis (GSEA) was conducted using ReactomeFIViz (https://reactome.org/tools/reactome-fiviz)
194 (Wu et al., 2014), a Cytoscape application for pathway and network-based data analysis. The
195 Search Tool for the Retrieval of Interacting Genes/Proteins (STRING) local network cluster
196 enrichment analysis was conducted using STRING database (http://string-db.org), which provides
197 a critical assessment and integration of protein-protein interaction (PPI), including direct
198 (physical) and indirect (functional) associations in a given organism (Szklarczyk et al., 2019).
199

200 **Measures of IFN activity**

201 MDBK cells (ATCC, CCL-22) were cultured in Eagle's Minimum Essential Medium (EMEM)
202 containing 10% heat-inactivated fetal bovine serum (FBS) and 50 μg/ml gentamicin (Rubinstein
203 et al., 1981). Vesicular stomatitis virus (VSV Indiana laboratory strain) (V-520-001-522, ATCC,
204 VR-1238) was passaged on Vero cells (ATCC, CCL-81), and viral titer was determined using the

205 plaque assay in Vero cells. MDBK cells bind and respond to human type I IFNs, α and β, but not
206 IFN-gamma (IFN-γ) (Rubinstein et al., 1981). Culture supernatants were collected from virus-
207 exposed MDMs on days 1, 3, and 5 following infection with SARS-CoV-2 at MOI of 0.01, then
208 assessed for IFN-α/β activity by protection against the VSV-induced cytopathicity measured in
209 MDBK cells (Rubinstein et al., 1981). Polyinosinic-polycytidylic acid (poly(I:C); Sigma-Aldrich,
210 P9582) served as a positive control for IFN induction via TLR3 engagement (Field et al., 1967).
211 Recombinant human IFN-α (PBL Assay Science, 11200-2) was used as assay standard. We also
212 investigated IFN activity upon the challenge of Teflon flask-suspended monocytes with SARS-
213 CoV-2 (MOI=0.01), before and after treatment of cells with 100 μg/ml poly(I:C).
214
215 **Western blot analysis**
216 At days 1, 3, and 5 after infection, MDMs were collected, and total protein was extracted using
217 lysis buffer containing 0.1% SDS, 100 mM Tris-HCL, 150 mM NaCl, 1 mM EDTA, 1% Triton
218 X-100, supplemented with protease and phosphatase inhibitor cocktail (Sigma-Aldrich, PPC1010).
219 Protein concentration was determined utilizing Pierce 660 Protein Assay kit (Thermo Fisher
220 Scientific, 22662) with ionic detergent compatibility reagent (Thermo Fisher Scientific, 22663)
221 following the manufacturer's instructions. Protein lysates (25 μg) were resolved by SDS-PAGE
222 and transferred to Immobilon-P PVDF membrane (Sigma-Aldrich, IPVH00010). Membranes were
223 blocked in 5% nonfat milk in TBST buffer at room temperature for 1 hour, followed by incubation
224 with primary antibodies to IFN-α (1:500, Thermo Fisher Scientific, MA5-37518), IFN-β (1:1000,
225 Abcam, ab85803), and β-actin (1:3000, Sigma-Aldrich, A3854) at 4°C overnight, followed by 1
226 hour incubation in 3% nonfat milk in Tris-buffered saline with 0.1% Tween 20 detergent
227 (TBST) buffer with horseradish peroxidase-conjugated anti-rabbit (1:2000, R&D Systems,

228 HAF008) or mouse (1:2000, R&D Systems, HAF018) secondary antibody. Immunoreactive bands
229 were detected using SuperSignal West Pico Chemiluminescent substrate (Thermo Fisher
230 Scientific, 34080), and images were captured using an iBright CL750 Imager (Thermo Fisher
231 Scientific). Immunoblots were quantified using ImageJ software (NIH) relative to β-actin
232 expression.
233
234 **Proteomic analysis**
235 On days 1, 3, and 5 post-infection, MDMs were collected, lysed with 2% SDS in 100 mM Tris-
236 HCL and 100 mM dithiothreitol, pH 7.6, and supplemented with protease and phosphatase
237 inhibitors. Protein concentration was determined using Pierce 660 Protein Assay kit with ionic
238 detergent compatibility reagent according to the manufacturer's instructions. Afterward, samples
239 were processed as previously described (Arainga et al., 2015) using filter-aided sample preparation
240 (FASP, Pall Life Sciences, OD010C34) for digestion of 50 μg per sample. Following overnight
241 digestion, samples were cleaned using the Oasis MCX column (Waters, 186000252) and C18 Zip-
242 Tips (Sigma-Aldrich, ZTC18M960). Cleaned peptides were quantitated using NanoDrop2000 at
243 205 nm. Following resuspension in 0.1% formic acid, 2 μg of the sample was used for label-free
244 quantification (LFQ) in UNMC Mass Spectrometry and Proteomics Core Facility as previously
245 described (Gao et al., 2020). Proteins identified by mass spectrometry were quantified to determine
246 differentially expressed proteins between mock and SARS-CoV-2-challenged MDMs at different
247 time points post-infection. Statistical analysis for proteomic data was performed using ANOVA,
248 and false discovery rate (FDR) for pathway analysis was controlled using the Benjamini-Hochberg
249 (BH) method (Benjamini and Hochberg, 1995). A protein was considered to be differentially
250 expressed if p value ≤ 0.05 and the absolute value of fold change ≥ 2. Next, functional and pathway

251 enrichment analysis of differentially expressed proteins in SARS-CoV-2-challenged MDMs
252 compared to mock-challenged MDMs was conducted at different times after virus challenge. Gene
253 enrichment analysis to identify immune system processes affected after virus exposure was
254 performed using Cytoscape in conjunction with the plug-in ClueGO (Bindea et al., 2009). GO
255 annotation, KEGG, Reactome GSEA, and STRING analyses were conducted using GO Resource,
256 DAVID, ReactomeFIViz, and STRING databases, respectively.
257
258 **Statistical analysis**
259 Results are presented as the mean ± standard error of the mean (SEM). Student's t-test or one-way
260 ANOVA followed by Tukey's multiple comparison test was used to analyze differences in the
261 mean values between groups. P values ≤ 0.05 were considered statistically significant. Statistical
262 analysis was performed using GraphPad Prism 9.1.0 software (GraphPad Software, San Diego,
263 CA).
264
265 **Results**
266 **ACE2 receptor expression during human monocyte-macrophage maturation**
267 ACE inhibitors were used to upregulate the SARS-CoV-2 receptor ACE2 and potentiate cell entry
268 (Ferrario et al., 2005; Pedrosa et al., 2021; Soler et al., 2009). As ACE inhibitors are frequently
269 prescribed to treat hypertension, we posit that they can increase susceptibility to SARS-CoV-2.
270 Therefore, we measured ACE2 expression on freshly isolated monocytes throughout cell isolation
271 and differentiation. Days 1, 3, 5, and 7 were evaluated for cells cultured with or without captopril,
272 an ACE inhibitor which is thought to increases ACE2 expression. In these studies, ACE2
273 expression by monocytes was found to peak by day 5 after initiation of cell differentiation then

274 decreased after that (**Figure 1A**), which corresponds to the susceptibility of infection of
275 monocytes-macrophages by other viruses (Gendelman et al., 1992; Lum et al., 2018;
276 Schmidtmayerova et al., 1996). On day 5, ACE2 expression increased by 23% in captopril-treated
277 cells. In parallel, the expression of phenotypic monocyte-macrophage surface markers, CD14 and
278 CD16, were not changed (**Figure 1A**). Based on these observations, we challenged MDMs with
279 SARS-CoV-2 on day 5 after start of cell differentiation and assessed whether captopril affects
280 susceptibility to infection.
281

282 **Abortive infection of MDMs is established following SARS-CoV-2 exposure**

283 To investigate whether human MDMs are susceptible to SARS-CoV-2 infection, monocytes were
284 isolated from healthy donors and differentiated in the presence or absence of captopril and infected
285 at day 5 after cell culture. The kinetic growth of SARS-CoV-2 in MDMs was determined from
286 culture supernatant tests of challenged cells over 10 days post-infection. In all studied groups
287 (captopril-treated and controls), the SARS-CoV-2 genome equivalent copies in the supernatant
288 significantly decreased during 5 days of viral exposure, becoming undetectable after that (**Figure**
289 **1B**). Additionally, the number of genome copies did not change significantly with or without
290 captopril. These results demonstrated that SARS-CoV-2 infection of human MDMs was abortive
291 and differentiated monocytes could not generate progeny virus in contrast to productive infection
292 of SARS-CoV-2 in Vero.STAT1 KO cells (**Figure 1B**). Our data also indicated that captopril did
293 not alter the susceptibility of MDMs to SARS-CoV-2 infection.
294

295 **Ultrastructural features of SARS-CoV-2-challenged MDMs**

296 Viral particles and mock and SARS-CoV-2-challenged MDMs were fixed at different time points

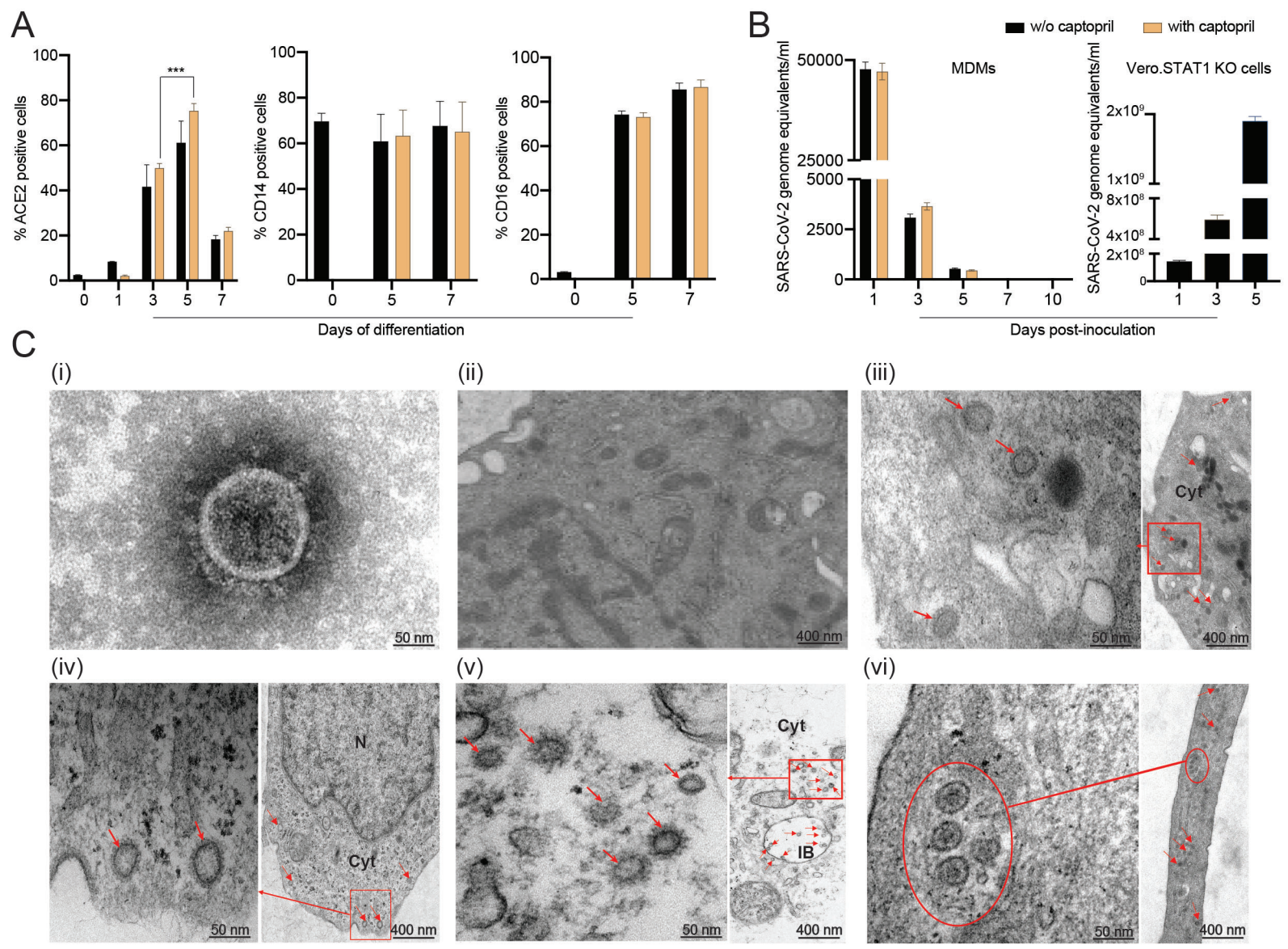
A
% ACE2 positive cells
% CD14 positive cells
% CD16 positive cells
***
Days of differentiation
B
w/o captopril
with captopril
MDMs
Vero.STAT1 KO cells
SARS-CoV-2 genome equivalents/ml
Days post-inoculation
C
(i)
(ii)
(iii)
(iv)
(v)
(vi)
50 nm
400 nm
Cyt
N
IB

297 **Figure 1. SARS-CoV-2 abortive infection of human MDMs.** (A) Expression of SARS-CoV-2
298 cell entry receptor ACE2 and phenotypic surface markers CD14 and CD16, during differentiation
299 of monocytes into macrophages, was analyzed by flow cytometry in absence or presence of
300 captopril. (B) SARS-CoV-2 presence in MDMs. SARS-CoV-2 (MOI=0.01) was used to infect
301 MDMs (with or without captopril). The number of virus genome equivalents per ml was measured
302 in the culture supernatant by RT-qPCR. Vero.STAT1 KO cells served as a positive control. (C)
303 Transmission electron micrographs of SARS-CoV-2-challenged MDMs. (C.i) A viral particle
304 from a pool of SARS-CoV-2 used for the virus challenges. Mock (C.ii) and SARS-CoV-2-
305 challenged MDMs (C.iii: day 1, C.iv: day 3, C.v: day 5, and C.vi: day 14 after viral exposure).
306 Red arrows and boxes demonstrate virus particles inside inclusion bodies and within the
307 macrophage cytoplasm. All experiments were done at least twice with representative images
308 depicted here. (**A** and **B**) Data are represented as mean ± SEM (n=3-6). Statistical significance
309 between groups was determined using unpaired Student's t-test or one-way ANOVA, and $p < 0.05$
310 was considered significant (*** $p < 0.001$). Abbreviations: w/o: without; Cyt: cytoplasm; N:
311 nucleus; IB: inclusion body. Scale bars: 50 nm (i and left panels of iii, iv, v, and vi) and 400 nm
312 (ii and right panels of iii, iv, v, and vi).

313

314 after viral exposure and then examined by TEM to determine ultrastructural changes in the virus-
315 challenged cells (**Figure 1C.i-vi**). Negative stain TEM shows the ultrastructure of a viral particle
316 from a pool of SARS-CoV-2 used for the virus challenges (**Figure 1C.i**). TEM analysis of mock-
317 treated cells showed normal architecture (**Figure 1C.ii**). By days 1 and 3 after exposure, viral
318 particles were observed inside the cytoplasm of many cells **(Figures 1C.iii** and **1C.iv)**. Five days
319 after viral exposure, an increased number of virions were observed inside inclusion bodies and cell
320 cytoplasm (**Figure 1C.v**). Surprisingly, while no viral genome copies were detected after 5 days
321 (**Figure 1B**), mature virions were observed 14 days after initial exposure (**Figure 1C.vi**). These
322 underly the persistence of virus in macrophages despite evidence of abortive infection.

323

324 **Abortive SARS-CoV-2 infection induces pro-inflammatory factors, but not IFN**

325 To investigate alterations in macrophage-mediated innate immune responses after SARS-CoV-2
326 exposure, a total of 84 key genes were examined. Transcriptional changes linked to immunity were
327 screened using RT^2 Profiler Human Innate and Adaptive Immune Response Array. Expression of

328 immune response genes in SARS-CoV-2-challenged MDMs were investigated against control
329 "mock-challenged cells" on days 1, 3, and 5 (**Supplementary Figure 1**). On day 1, more than two-
330 fold increase in expression of pro-inflammatory cytokine and chemokine genes were detected,
331 including *IL-6, TNF-α, IL-1α, IL17A, IL8*, colony-stimulating factor 2 (*CSF2*), chemokine (C-C
332 motif) ligand 2 (*CCL2*), and *CCL5*. Interestingly, on day 3, gene expression of the node-like
333 receptor family pyrin domain containing 3 (*NLRP3*) and *IL-1β* increased by 8.84- and 5.64-fold,
334 respectively. On day 5, expression for these pro-inflammatory cytokines and chemokines were at
335 baseline or decreased with the exception of *IL-6* and *CCL2*. Gene expression of anti-inflammatory
336 cytokine *IL-10* was elevated on days 1 and 5 supporting the attenuation of pro-inflammatory
337 responses (Lu et al., 2021). Importantly, expression of IFN-linked genes *IFN-α1, IFN-β1, IFN-γ*,
338 IFN regulatory factor 7 (*IRF7*), and tyrosine kinase 2 (*TYK2*) genes increased on day 1 but returned
339 to near baseline by days 3 and 5. These data demonstrate a complex pro- and anti-inflammatory
340 network interactions that are sustained to day 5 with attenuated IFN responses following SARS-
341 CoV-2 exposure (**Figure 2A**).
342
343 **Functional and pathway enrichment of immune regulated genes**
344 SARS-CoV-2 infection may induce dynamic changes of immune-based gene expression in specific
345 cellular biological processes and pathways in virus-challenged cells. To assess these changes,
346 functional and pathway enrichment analyses were performed on immune-regulated genes screened
347 in SARS-CoV-2-challenged MDMs compared to controls at days 1, 3, and 5 (**Supplementary file**
348 **1**). Multiple immune processes were enriched upon viral exposure, including defense response to
349 other organism, positive regulation of immune system processes, cell surface receptor signaling
350 pathways, and positive regulation of immune responses (**Figure 2B**).

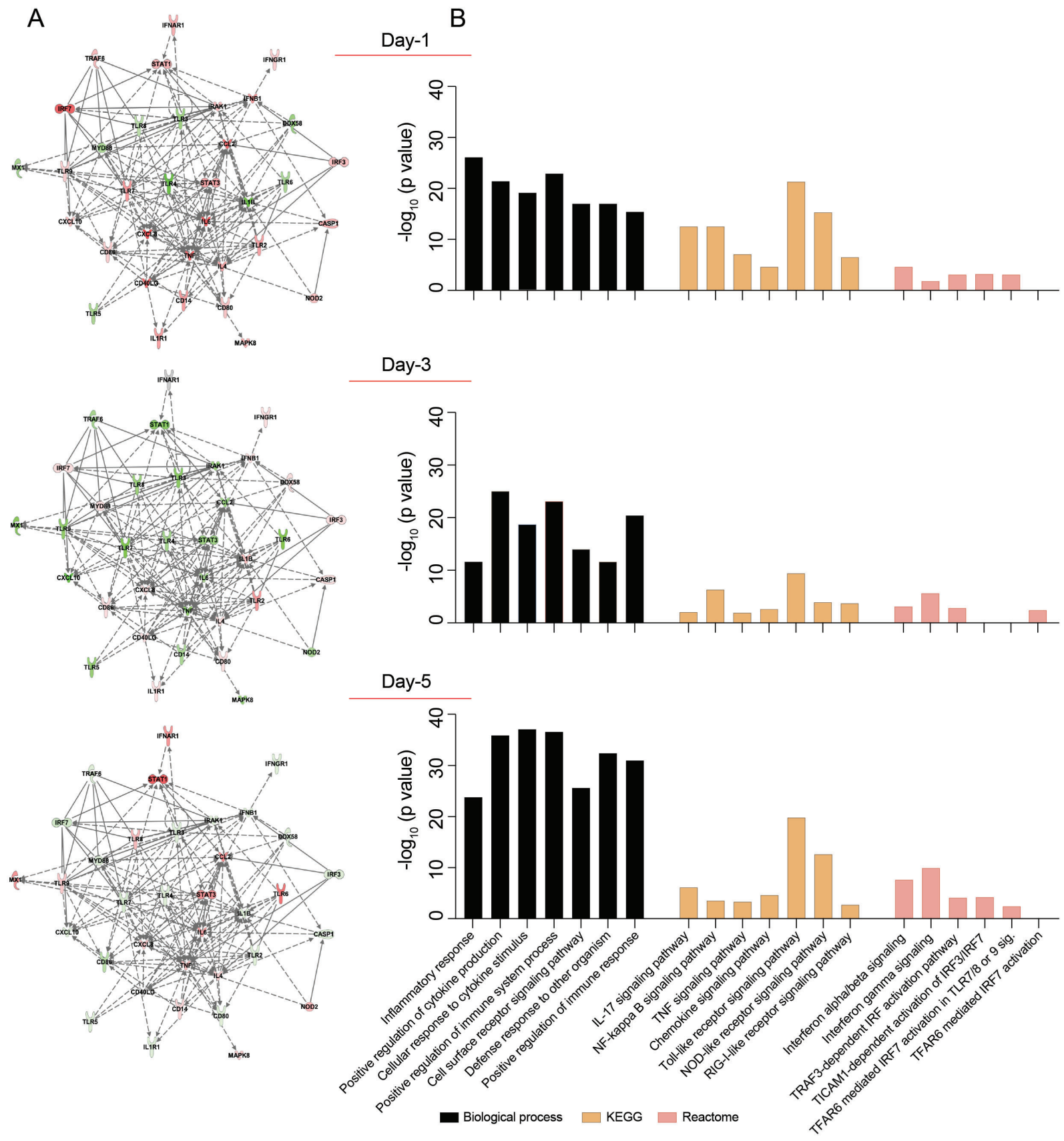
A
B
Day-1
Day-3
Day-5
-log10 (p value)
0
10
20
30
40
IFNAR1
IFNGR1
TRAF6
STAT1
IFNB1
IRAK1
IRF7
TLR8
TLR3
DDX58
MYD88
CCL2
IRF3
MX1
TLR9
TLR7
TLR4
STAT3
TLR6
IL1B
CXCL10
IL6
CASP1
CXCL8
TLR2
CD86
TNF
IL4
CD40LG
CD14
CD80
NOD2
TLR5
IL1R1
MAPK8
Inflammatory response
Positive regulation of cytokine production
Cellular response to cytokine stimulus
Positive regulation of immune system process
Cell surface receptor signaling pathway
Defense response to other organism
Positive regulation of immune response
IL-17 signaling pathway
NF-kappa B signaling pathway
TNF signaling pathway
Chemokine signaling pathway
Toll-like receptor signaling pathway
NOD-like receptor signaling pathway
RIG-I-like receptor signaling pathway
Interferon alpha/beta signaling
Interferon gamma signaling
TRAF3-dependent IRF activation pathway
TICAM1-dependent activation of IRF3/IRF7
TFAR6 mediated IRF7 activation in TLR7/8 or 9 sig.
TFAR6 mediated IRF7 activation
Biological process
KEGG
Reactome

351 **Figure 2. Transcriptomic profile of SARS-CoV-2-challenged MDMs.** Expression of 84 genes
352 specific for human innate and adaptive immune responses were screened in SARS-CoV-2-
353 challenged MDMs compared to mock-challenged MDMs at different times post-challenge, using
354 RT^2 Profiler Human Innate and Adaptive Immune Response 96-well Array. Fold changes in the
355 gene expression were determined via Qiagen's RT^2 Profiler analysis software (n=4). (A) IPA was
356 performed with upregulated or downregulated genes to identify putative network interactions
357 involved in SARS-CoV2-MDM interactions. Upregulated genes are shaded red with darker shade
358 indicating higher upregulation, while green shades denote downregulation in gene expression.
359 Solid grey lines indicate direct interactions, while dotted grey lines correspond to indirect
360 interactions. (B) Functional and pathway enrichment analysis of transcriptomic dataset was
361 performed using GO-term, KEGG, and Reactome analyses at different time points post-infection.
362 Different immune and inflammation-related biological processes and pathways affected in SARS-
363 CoV-2-challenged MDMs were plotted as a bar chart compared to mock-challenged MDMs.

364

365 All indicated they comprised activated immune responses in the virus-challenged MDMs. In
366 addition, a series of inflammation-related processes were enriched, including inflammatory
367 response, positive regulation of cytokine production, and cellular response to cytokine stimulus
368 (**Figure 2B**), highlighting inflammation responses induced after viral exposure. Similarly,
369 different immune and inflammation-related molecular functions such as cytokine activity,
370 chemokine activity, complement component C1q binding, type I IFN receptor binding, and IL-1
371 receptor binding were enriched after virus exposure (**Supplementary file 1**). Furthermore, KEGG
372 pathway analysis showed enrichment of TLR, NOD-like receptor, and RLR signaling pathways
373 (**Figure 2B**), suggesting the activation of PRRs on MDMs to recognize viral PAMPs initiating
374 innate immune responses. Moreover, KEGG pathway analysis depicted enrichment of IL-17, NF-
375 κB, TNF, and chemokine signaling pathways (**Figure 2B**), highlighting different inflammatory
376 pathways induced in the SARS-CoV-2-challenged MDMs. Interestingly, Reactome analysis
377 revealed enrichment of multiple IFN-related signaling pathways including IFN-α/β signaling, IFN-
378 γ signaling, TICAM1-dependent activation of IRF3/IRF7, TRAF3-dependent IRF activation
379 pathway, and TRAF6 mediated IRF7 activation (**Figure 2B**). In addition, immune and
380 inflammation-mediated molecular functions were enriched in virus-challenged cells

381 (**Supplementary file 1**). The interacting proteins involved in the screened innate and adaptive
382 immune-related genes were also identified using STRING analysis of their interaction networks
383 (**Supplementary file 1**).
384
385 **SARS-CoV-2 monocyte-macrophage engagement and failed induction of IFN activity**
386 To determine whether exposure to the SARS-CoV-2 can trigger antiviral IFN activities in human
387 macrophages, culture supernatants were collected at different times post-viral exposure and
388 assayed in VSV-challenged MDBK cells. Notably, no type I IFN activity was observed in SARS-
389 CoV-2-challenged MDM cultures at different time intervals following viral challenge (**Figure**
390 **3A).** These data stand in contrast to the transcriptomic results, which displayed increases in IFN
391 pathway-linked genes. Furthermore, no additive or synergistic IFN activity was detected in control
392 and SARS-CoV-2-challenged monocytes treated with poly(I:C) (**Figure 3B**). Taken together, the
393 data demonstrate that SARS-CoV-2-MDM interactions do not affect IFN activities. To affirm this,
394 we evaluated the protein expression level of IFN-α and IFN-β in SARS-CoV-2 exposed MDMs at
395 days 1, 3, and 5 post-exposure. Similar to IFN activity, no IFN-α or IFN-β proteins were produced
396 in the SARS-CoV-2-challenged MDMs (**Figure 3C**). Altogether, our data demonstrate that SARS-
397 CoV-2 exposure of MDM does not trigger IFN activity or protein production in human monocytes-
398 macrophages.
399
400 **Proteomic profiles of SARS-CoV-2-challenged MDMs**
401 In attempts to elucidate the mechanisms of the MDM response against the SARS-CoV-2 challenge,
402 we obtained the proteome profiles from lysates of viral exposed macrophages and compared those
403 to non-exposed counterparts. On defined days after viral exposure, the expression of more than

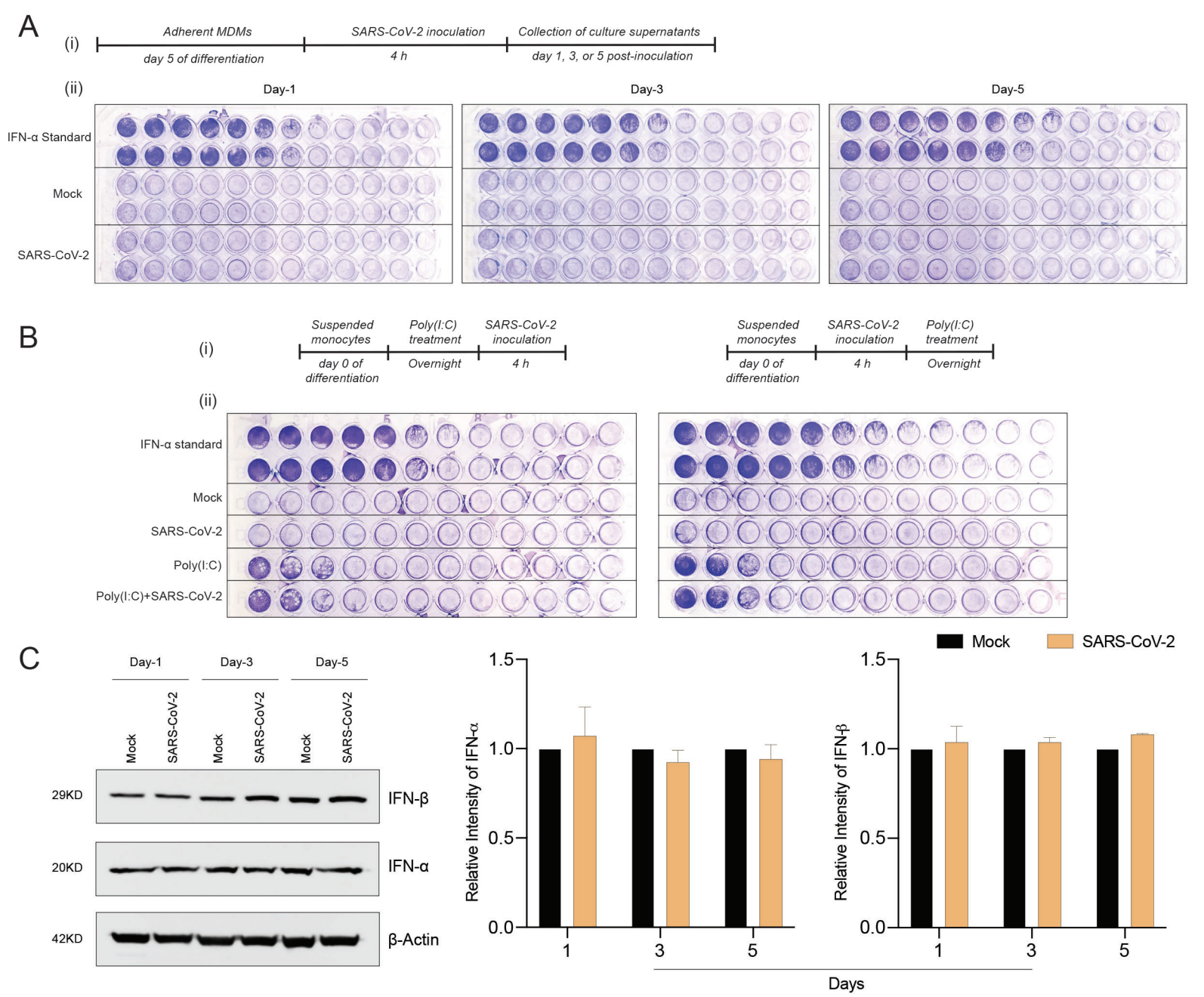
A
(i)
Adherent MDMs
day 5 of differentiation
SARS-CoV-2 inoculation
4 h
Collection of culture supernatants
day 1, 3, or 5 post-inoculation
(ii)
Day-1
Day-3
Day-5
IFN-α Standard
Mock
SARS-CoV-2
B
(i)
Suspended monocytes
day 0 of differentiation
Poly(I:C) treatment
Overnight
SARS-CoV-2 inoculation
4 h
Suspended monocytes
day 0 of differentiation
SARS-CoV-2 inoculation
4 h
Poly(I:C) treatment
Overnight
(ii)
IFN-α standard
Mock
SARS-CoV-2
Poly(I:C)
Poly(I:C)+SARS-CoV-2
C
Day-1
Day-3
Day-5
Mock
SARS-CoV-2
Mock
SARS-CoV-2
Mock
SARS-CoV-2
29KD
IFN-β
20KD
IFN-α
42KD
β-Actin
Mock
SARS-CoV-2
Relative Intensity of IFN-α
Relative Intensity of IFN-β
1.5
1.0
0.5
0.0
1
3
5
Days

Figure 3. SARS-CoV-2 does not induce IFN activity in monocytes-macrophages. (A) MDMs were infected with SARS-CoV-2 (MOI=0.01) and the culture supernatants were collected at days 1, 3, and 5 post-infection. The collected culture supernatants were used to assess IFN activity in VSV-challenged bovine MDBK cells. Recombinant human IFN-α was used as standard. (A.i) Experimental timeline. (A.ii) Representative images of IFN activity assay plates. (B) No additive or synergistic responses in poly(I:C)-induced IFN activity between control and SARS-CoV-2-challenged monocytes. Suspended monocytes were treated with 100 μg poly(I:C) overnight before or after the infection with SARS-CoV-2 (MOI=0.01) for 4 h. (B.i) Experimental timeline. (B.ii) Representative images of IFN activity assay plates. (C) Western blot analysis was performed to determine expression of IFN-α and IFN-β in cell lysates at different times after viral exposure. Representative immunoblot and densitometric quantification are shown. All experiments were done at least twice, and one representative image is shown. (C) Data represent mean ± SEM (n=3). Statistical significance between the groups was determined with unpaired Student's t-test and $p < 0.05$ was considered significant.

4,000 proteins were identified and quantified using differential proteomic tests. Amongst total identified proteins, 1776, 1372, and 2448 proteins were significantly differentially expressed ($p \leq 0.05$ and fold change ≥ 2), on days 1, 3, and 5, respectively, after viral challenge (**Supplementary file 2**). Volcano plots depicting differentially expressed proteins in SARS-CoV-2-challenged MDMs compared to controls are shown in **Supplementary Figure 2**. To obtain a detailed understanding of changes in the MDM proteomic profile after viral challenge, we performed functional and pathway enrichment analyses of differentially regulated proteins in virus-challenged MDMs at different times. Amongst total proteins altered on day 1, only 5% were involved in negative regulation of inflammatory response to an antigenic stimulus. In contrast, on days 3 and 5, 38.1% and 23.53% of altered proteins, respectively, belonged to myeloid cell activation involved in immune responses (**Figure 4A**). Immune processes of each function indicated in pie charts include, but are not limited to, activation of the innate immune response, myeloid cell activation, innate immune response activating signal transduction, and innate immune response activating cell surface receptor signaling pathway (**Figure 4A** and **Supplementary file 3**). All indicated activated immune and inflammatory responses in MDMs upon viral challenge.

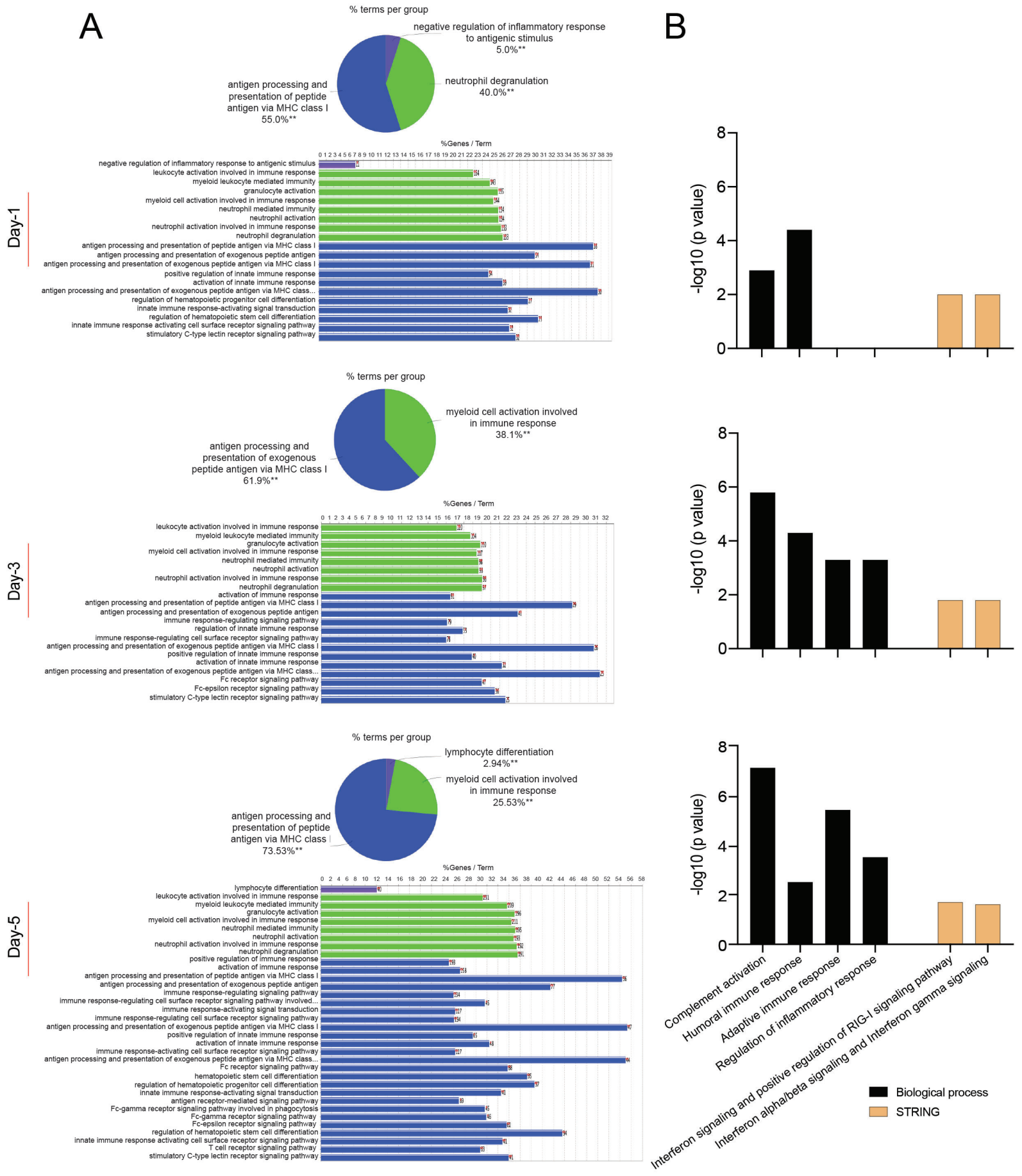
A
B
% terms per group
negative regulation of inflammatory response to antigenic stimulus 5.0%**
neutrophil degranulation 40.0%**
antigen processing and presentation of peptide antigen via MHC class I 55.0%**
%Genes / Term
Day-1
negative regulation of inflammatory response to antigenic stimulus
leukocyte activation involved in immune response
myeloid leukocyte mediated immunity
granulocyte activation
myeloid cell activation involved in immune response
neutrophil mediated immunity
neutrophil activation
neutrophil activation involved in immune response
neutrophil degranulation
antigen processing and presentation of peptide antigen via MHC class I
antigen processing and presentation of exogenous peptide antigen
antigen processing and presentation of exogenous peptide antigen via MHC class I
positive regulation of innate immune response
activation of innate immune response
antigen processing and presentation of exogenous peptide antigen via MHC class...
regulation of hematopoietic progenitor cell differentiation
innate immune response-activating signal transduction
regulation of hematopoietic stem cell differentiation
innate immune response activating cell surface receptor signaling pathway
stimulatory C-type lectin receptor signaling pathway
% terms per group
myeloid cell activation involved in immune response 38.1%**
antigen processing and presentation of exogenous peptide antigen via MHC class I 61.9%**
%Genes / Term
Day-3
leukocyte activation involved in immune response
myeloid leukocyte mediated immunity
granulocyte activation
myeloid cell activation involved in immune response
neutrophil mediated immunity
neutrophil activation
neutrophil activation involved in immune response
neutrophil degranulation
activation of immune response
antigen processing and presentation of peptide antigen via MHC class I
antigen processing and presentation of exogenous peptide antigen
immune response-regulating signaling pathway
regulation of innate immune response
immune response-regulating cell surface receptor signaling pathway
antigen processing and presentation of exogenous peptide antigen via MHC class I
positive regulation of innate immune response
activation of innate immune response
antigen processing and presentation of exogenous peptide antigen via MHC class...
Fc receptor signaling pathway
Fc-epsilon receptor signaling pathway
stimulatory C-type lectin receptor signaling pathway
% terms per group
lymphocyte differentiation 2.94%**
myeloid cell activation involved in immune response 25.53%**
antigen processing and presentation of peptide antigen via MHC class I 73.53%**
%Genes / Term
Day-5
lymphocyte differentiation
leukocyte activation involved in immune response
myeloid leukocyte mediated immunity
granulocyte activation
myeloid cell activation involved in immune response
neutrophil mediated immunity
neutrophil activation
neutrophil activation involved in immune response
neutrophil degranulation
positive regulation of immune response
activation of immune response
antigen processing and presentation of peptide antigen via MHC class I
antigen processing and presentation of exogenous peptide antigen
immune response-regulating signaling pathway
immune response-regulating cell surface receptor signaling pathway involved...
immune response-activating signal transduction
immune response-regulating cell surface receptor signaling pathway
antigen processing and presentation of exogenous peptide antigen via MHC class I
positive regulation of innate immune response
activation of innate immune response
immune response-activating cell surface receptor signaling pathway
antigen processing and presentation of exogenous peptide antigen via MHC class...
Fc receptor signaling pathway
hematopoietic stem cell differentiation
regulation of hematopoietic progenitor cell differentiation
innate immune response-activating signal transduction
antigen receptor-mediated signaling pathway
Fc-gamma receptor signaling pathway involved in phagocytosis
Fc-gamma receptor signaling pathway
Fc-epsilon receptor signaling pathway
regulation of hematopoietic stem cell differentiation
innate immune response activating cell surface receptor signaling pathway
T cell receptor signaling pathway
stimulatory C-type lectin receptor signaling pathway
-log10 (p value)
Complement activation
Humoral immune response
Adaptive immune response
Regulation of inflammatory response
Interferon signaling and positive regulation of RIG-I signaling pathway
Interferon alpha/beta signaling and Interferon gamma signaling
Biological process
STRING

434 **Figure 4. Proteomic profile of SARS-CoV-2-challenged MDMs.** (A) Gene enrichment analysis
435 was performed using Cytoscape in conjunction with the plug-in ClueGO at different times after
436 viral exposure. Pie charts representing the distribution of identified differentially expressed
437 proteins according to observed immune processes and bar charts demonstrating the specific
438 processes that correspond to their classification. The same color key used in the pie charts applied
439 in the bar charts. (B) Functional and pathway enrichment analyses of proteomic dataset were
440 performed using GO annotation, KEGG, Reactome GSEA, and STRING analyses at different time
441 points post-infection. Different immune-related biological processes and PPI networks affected in
442 SARS-CoV-2-challenged MDMs were plotted as a bar chart compared to mock-challenged
443 MDMs.

444

445 Additionally, viral exposure induced changes in biological processes related to the endoplasmic
446 reticulum (ER) and mRNA on days 1 and 3 after challenge. With positive fold changes, the
447 enriched biological processes included protein localization to ER, protein targeting to ER,
448 regulation of mRNA metabolic process, nuclear-transcribed mRNA catabolic process, and mRNA
449 splicing via spliceosome (**Supplementary file 4**). Similarly, on days 1 and 3 after viral challenge,
450 Reactome analysis depicted enrichment of processes related to RNA processing, with positive fold
451 change, including rRNA processing in the nucleus and cytosol and mRNA splicing
452 (**Supplementary file 4**). Moreover, KEGG pathway analysis showed an enrichment of ribosome
453 function as a pathway of genetic information processing and translation on day 1. Similarly, the
454 molecular function of a structural constituent of the ribosome was enriched with positive fold
455 change on day 1 (**Supplementary file 4**). Interestingly, GO-term analysis showed robust
456 enrichment of different immune responses such as complement activation, humoral immune
457 response, adaptive immune response, and regulation of inflammatory response with negative fold
458 changes suggesting dysregulated immune responses to SARS-CoV-2 in MDMs (**Figure 4B**).
459 Importantly, STRING analysis of PPIs showed enrichment of IFN-related interaction networks
460 such as "IFN signaling and positive regulation of RIG-I signaling pathway" and "IFN-α/β
461 signaling and IFN-γ signaling", with negative fold changes, suggesting dysregulated IFN

462 responses induced by SARS-CoV-2 (**Figure 4C** and **Supplementary file 4**). Overall, these results
463 support transcriptomic, IFN activity, and protein evaluations that demonstrated attenuated IFN
464 responses in SARS-CoV-2-challenged MDMs.
465
466 **Discussion**
467 MPs are the first line of host defense against viral infection (Nikitina et al., 2018). These sentinel
468 cells interact with SARS-CoV-2 to define COVID-19 pathogenesis. That includes, but is not
469 limited to, CSS, ARDS, and multiorgan dysfunction (Guan et al., 2020). As a first line defense
470 mechanism, the initial virus-MP interaction following the entry of the pathogenic virus into host
471 cells represents a critical determinant for infectivity and pathogenesis (Li, 2016; Perlman and
472 Netland, 2009; Shang et al., 2020). To this end, we have better defined such virus-host cell
473 interactions and determined relationships between ACE2 receptor expression and monocyte-
474 macrophage differentiation during abortive SARS-CoV-2 infection. Like other viral infections, we
475 reasoned that monocytes would respond with an elevated expression of pro-inflammatory
476 molecules and antiviral responses. Indeed, this has already been reported for influenza,
477 Chikungunya, herpes, Zika, and lentiviral infections that include human immunodeficiency virus
478 type one (HIV-1) and herpes viruses (Coates et al., 2018; Her et al., 2010; Krzyzowska et al., 2013;
479 Lum et al., 2018; Schmidtmayerova et al., 1996). Each elicits profound inflammation during early
480 viral infection. However, unlike other known viral infections, SARS-CoV-2 infection is abortive
481 and balances pro- and anti-inflammatory processes with a unique cell signature. The resulting
482 signature defines the pathways towards the major cause for morbidity and mortality in COVID-
483 19: the CSS leading to ARDS and other multi-organ failures. The specific lack of induction of IFN

484 also serves to define a specific monocyte-macrophage-virus phenotype during both early and
485 progressive infection (Dalskov et al., 2020; Yang et al., 2020).
486
487 Herein, we show increased expression of viral receptor ACE2 during monocyte-macrophage
488 differentiation. Interestingly, further induction of ACE2 expression by captopril, a well-known
489 ACE inhibitor, was observed. Captopril induces a reduction of angiotensin II, which increases
490 ACE2 expression and activity. This occurs through angiotensin type 1 receptor-dependent ACE2
491 internalization followed by lysosomal degradation (Deshotels et al., 2014). However, the observed
492 upregulation of ACE2 expression failed to affect infection with SARS-CoV-2. Despite infection
493 of MDMs with SARS-CoV-2 when ACE2 receptor expression peaked, the infection remained
494 abortive in agreement with prior reports (Boumaza et al., 2021; Yang et al., 2020; Zheng et al.,
495 2021). The inability of captopril to increase the susceptibility of MDM infection with SARS-CoV-
496 2 is in accordance with a recent study indicating that treatment of human alveolar type-II
497 pneumocytes with captopril induced upregulation of ACE2 expression and counteracted drug-
498 induced reduction of SARS-CoV-2 spike protein entry (Pedrosa et al., 2021). This occurred
499 through inhibition of A disintegrin and metalloprotease 17 (ADAM17), which has been shown to
500 play an essential role in ACE2 shedding and viral entry into the cells (Lambert et al., 2005).
501 Nonetheless, viral particles were present inside cytoplasmic structures of macrophages up to two
502 weeks after the viral challenge underscoring any continuity of immune responses.
503
504 SARS-CoV-2 abortive infection likely results from intracellular mechanisms induced upon MP
505 activation. Human coronaviruses can infect human peripheral blood mononuclear cells leading to
506 cell activation and aberrant production of pro-inflammatory mediators with increased

507 chemoattraction (Channappanavar and Perlman, 2017; Yilla et al., 2005; Zhou et al., 2014). In
508 particular, virus-exposed monocytes-macrophages can serve as perpetrators for virus-induced
509 inflammatory responses within different body organs, as seen by the abundance of pro-
510 inflammatory macrophages in bronchoalveolar lavage fluid obtained from severe COVID-19 cases
511 (Liao et al., 2020). The MP pro-inflammatory factors can contribute to local tissue inflammation
512 and systemic inflammatory responses that characterize cytokine storm (Nikitina et al., 2018). In
513 the current study, the transcriptomic profile of SARS-CoV-2-challenged MDMs demonstrated
514 increased mRNA expression of multiple pro-inflammatory molecules, including *IL-6, TNF-α, IL-*
515 *1α, IL17A, IL8, CSF2, CCL2, CCL5, NLRP3,* and *IL-1β* upon the virus exposure. Our data
516 confirmed previous reports which showed excessive production of pro-inflammatory cytokines
517 and chemokines in the SARS-CoV-2-exposed MPs (Boumaza et al., 2021; Yang et al., 2020;
518 Zheng et al., 2021). In parallel, our data displayed enrichment of different inflammation-related
519 pathways such as IL-17, NF-κB, and TNF signaling pathways, following viral exposure. IL-17 is
520 known for its pivotal role in inducing and mediating pro-inflammatory responses and its
521 involvement in different inflammatory autoimmune diseases (Kuwabara et al., 2017). NF-κB
522 serves as a central mediator of inflammation since the DNA binding site for NF-κB was found in
523 the promoter regions of multiple pro-inflammatory molecules (Hayden and Ghosh, 2004). Thus,
524 the activation of NF-κB with other pro-inflammatory transcription factors leads to the transcription
525 of several pro-inflammatory molecules such as IL-1β, inducible nitric oxide synthase (iNOS), and
526 TNF-α (Dasgupta et al., 2003; Liu et al., 2002). In addition, the transcriptome of SARS-CoV-2-
527 challenged MDMs showed enrichment of multiple immune-related biological processes,
528 molecular functions, and signaling pathways such as positive regulation of immune response, cell
529 surface receptor signaling pathway, cytokine activity, chemokine activity, TLR signaling pathway,

530 and NOD-like receptor signaling pathway, demonstrating cell activation of MDMs after viral
531 exposure. Notably, the proteome of virus-challenged macrophages revealed the dysregulation of
532 different immune processes such as regulation of inflammatory response, complement activation,
533 and linked adaptive and humoral immune responses. Overall, our findings demonstrate MDM
534 activation by SARS-CoV-2 is associated with exaggerated inflammatory responses and
535 dysregulated immune activities.
536
537 Significantly, SARS-CoV-2 induced an attenuated MP IFN response, as the transcript expression
538 of type I (IFN-α1 and IFN-β1) and type II (IFN-γ) IFNs in the virus-challenged cells increased
539 early after exposure but returned to or below normal levels at later times. Our findings are
540 consistent with previous reports depicting a dysregulated IFN response in SARS-CoV-2-
541 challenged MDMs and alveolar macrophages (Dalskov et al., 2020; Yang et al., 2020). This
542 attenuated IFN response provides a possible mechanism for delayed viral clearance from cells up
543 to two weeks after inoculation. Similarly, our study showed the inability of SARS-CoV-2 to induce
544 IFN activity or production in MDMs, as illustrated by the failure of culture supernatants of infected
545 cells to provide protection against the cytopathic effects induced by VSV in MDBK cells as well
546 as unchanged levels of IFN-α and IFN-β after the virus challenge. These findings are following a
547 recent study that demonstrated the absence of IFN induction in the alveolar macrophages
548 challenged with SARS-CoV-2 (Dalskov et al., 2020). A possible explanation is the presence of a
549 cap structure on the viral genome. The *Coronoviridae* family contains this structure enabling the
550 virus to evade recognition by PRRs and prevent the host innate immune response mediated by the
551 RIG-I/mitochondrial antiviral-signaling (MAVS) pathway that recognizes single-stranded RNAs
552 without a cap structure (Chen and Guo, 2016; Pichlmair et al., 2006). Moreover, different SARS-

553 CoV-2 proteins were found to antagonize type I IFN production through other mechanisms (Xia
554 et al., 2020). SARS-CoV-2 nonstructural protein 6 (nsp6) binds TANK binding kinase 1 (TBK1)
555 to suppress IRF3 phosphorylation, and nsp13 binds and blocks TBK1 phosphorylation. In addition,
556 open reading frame 6 (ORF6) binds importin Karyopherin α 2 to inhibit IRF3 nuclear
557 translocation, and ORF7b prevents STAT1 phosphorylation and nuclear translocation,
558 consequently inhibiting the transcription of multiple IFN stimulated genes (ISGs) which possess
559 antiviral functions (Xia et al., 2020). In parallel, the negative fold change of IFN-related interaction
560 networks: "IFN signaling and positive regulation of RIG-I signaling pathway" and "IFN-α/β
561 signaling and IFN-γ signaling" indicates dysregulated IFN responses in the SARS-CoV-2-
562 challenged MDMs. Thus far, our data suggest an aberrant IFN response induced by SARS-CoV-2
563 in human MDMs. Early IFN induction was halted at the transcriptional level one day post-infection
564 and did not proceed to the translational level. Thus, we postulate that aberrant IFN responses in
565 the face of a robust inflammatory environment presage a lack of viral infection control and
566 multiorgan damage in COVID-19 (Gavriatopoulou et al., 2020).
567
568 In summary, we demonstrate that abortive SARS-CoV-2 macrophage infection triggers a unique
569 signature of inflammatory responses. This includes combinations of abortive infection with
570 delayed viral clearance, excessive pro-inflammatory cytokine and chemokine productions, and
571 attenuated IFN responses. Each and all imply dysfunction of the innate immune system after viral
572 exposure. Transcriptomic and proteomic profiles of SARS-CoV-2-challenged MPs provide
573 signatures for understanding COVID-19 pathogenesis. The lack of adequate antiviral innate
574 immune responses in the midst of cytokine storm heralds an absence of viral infection control that

575 exacerbates clinical manifestations and contributes to end-organ damage for COVID-19-related
576 morbidities and mortalities.
577
578 **Conflict of interest**
579 Howard E. Gendelman is a co-founder of Exavir Therapeutics, Inc. who is developing antiviral
580 and elimination therapies for HIV/AIDS and other viral infections.
581
582 **Acknowledgments**
583 The authors thank the UNMC Elutriation and Cell Separation Core Facility (Myhanh Che and Na
584 Ly) for providing human monocytes. The authors would also like to thank Dr. Pawel Ciborowski
585 and his research group within the Department of Pharmacology and Experimental Neuroscience
586 at UNMC for discussion and assistance with the proteomic sample preparation. The authors
587 acknowledge the UNMC Mass Spectrometry and Proteomics Core Facility for assistance with the
588 proteomic analysis. The authors would also like to acknowledge the UNMC Flow Cytometry
589 Research Core Facility for assistance with the flow cytometric analysis. The authors would like to
590 thank Dirk Anderson (The Biotech Microscopy Core Research Facility of University of Nebraska-
591 Lincoln) for his assistance with TEM sample preparations.
592
593 **Funding**
594 The work was supported, in part, by the University of Nebraska Foundation, which includes
595 donations from the Carol Swarts, M.D. Emerging Neuroscience Research Laboratory, the
596 Margaret R. Larson Professorship, the Frances and Louie Blumkin, and the Harriet Singer
597 Research Donations. We thank Dr. Bradley Britigan, Dean of the College of Medicine at UNMC,

598 for providing funds to support the SARS-CoV-2 studies. The research also received support from
599 National Institutes of Health grants PO1 DA028555, R01 NS36126, PO1 MH64570, P30
600 MH062261, P20 GM113126, R01 AG043540, and 2R01 NS034239. We also thank the INBRE
601 grant support from 2P20GM103427 for infrastructure research support.
602

603 **Author contributions**

604 M.M.A.: Investigation, Methodology, Validation, Visualization, Formal analysis, Data curation,
605 Writing-original draft, review and editing; P.Y.: Investigation, Methodology, Formal analysis,
606 Data curation, Writing-review and editing; J.M.: Investigation, Methodology, Data curation,
607 Writing-review and editing; K.E.O.: Validation, Visualization, Writing-review and editing; F.S.:
608 Investigation, Validation, Writing-review and editing; Y.Z.: Investigation, Validation, Data
609 curation, Writing-review and editing; L.J.: Investigation, Formal analysis, Writing-review and
610 editing; K.P.: Investigation, Validation, Writing-review and editing; A.A.: Investigation,
611 Validation, Visualization, Writing-review and editing; S.N.B.: Supervision, Visualization,
612 Writing-review and editing; R.L.M.: Conceptualization, Methodology, Supervision, Writing-
613 review and editing; H.E.G.: Conceptualization, Funding Acquisition, Methodology, Resources,
614 Supervision, Writing-original draft, review and editing; All authors have read and approved the
615 final version of the manuscript.
616
617

618 **References**
619

620 Arainga, M., Guo, D., Wiederin, J., Ciborowski, P., McMillan, J., and Gendelman, H. E. (2015).
621 Opposing regulation of endolysosomal pathways by long-acting nanoformulated
622 antiretroviral therapy and HIV-1 in human macrophages. *Retrovirology, 12*, 5.
623 doi:10.1186/s12977-014-0133-5
624 Benjamini, Y., and Hochberg, Y. (1995). Controlling the false discovery rate: A practical and
625 powerful approach to multiple testing. *Journal of the Royal Statistical Society: Series B*
626 *(Methodological),* *57*(1), 289-300. doi:https://doi.org/10.1111/j.2517-
627 6161.1995.tb02031.x
628 Bindea, G., Mlecnik, B., Hackl, H., Charoentong, P., Tosolini, M., Kirilovsky, A., Fridman, W.
629 H., Pages, F., Trajanoski, Z., and Galon, J. (2009). ClueGO: a Cytoscape plug-in to
630 decipher functionally grouped gene ontology and pathway annotation networks.
631 *Bioinformatics, 25*(8), 1091-1093. doi:10.1093/bioinformatics/btp101
632 Boumaza, A., Gay, L., Mezouar, S., Bestion, E., Diallo, A. B., Michel, M., Desnues, B., Raoult,
633 D., La Scola, B., Halfon, P., Vitte, J., Olive, D., and Mege, J. L. (2021). Monocytes and
634 macrophages, targets of SARS-CoV-2: the clue for Covid-19 immunoparalysis. *J Infect*
635 *Dis*. doi:10.1093/infdis/jiab044
636 Channappanavar, R., and Perlman, S. (2017). Pathogenic human coronavirus infections: causes
637 and consequences of cytokine storm and immunopathology. *Semin Immunopathol, 39*(5),
638 529-539. doi:10.1007/s00281-017-0629-x
639 Chen, Y., and Guo, D. (2016). Molecular mechanisms of coronavirus RNA capping and
640 methylation. *Virol Sin, 31*(1), 3-11. doi:10.1007/s12250-016-3726-4
641 Coates, B. M., Staricha, K. L., Koch, C. M., Cheng, Y., Shumaker, D. K., Budinger, G. R. S.,
642 Perlman, H., Misharin, A. V., and Ridge, K. M. (2018). Inflammatory monocytes drive
643 influenza A virus-mediated lung injury in juvenile mice. *J Immunol, 200*(7), 2391-2404.
644 doi:10.4049/jimmunol.1701543
645 Dalskov, L., Mohlenberg, M., Thyrsted, J., Blay-Cadanet, J., Poulsen, E. T., Folkersen, B. H.,
646 Skaarup, S. H., Olagnier, D., Reinert, L., Enghild, J. J., Hoffmann, H. J., Holm, C. K., and
647 Hartmann, R. (2020). SARS-CoV-2 evades immune detection in alveolar macrophages.
648 *EMBO Rep, 21*(12), e51252. doi:10.15252/embr.202051252

649 Dasgupta, S., Jana, M., Liu, X., and Pahan, K. (2003). Role of very-late antigen-4 (VLA-4) in
650 myelin basic protein-primed T cell contact-induced expression of proinflammatory
651 cytokines in microglial cells. *J Biol Chem, 278*(25), 22424-22431.
652 doi:10.1074/jbc.M301789200
653 Deshotels, M. R., Xia, H., Sriramula, S., Lazartigues, E., and Filipeanu, C. M. (2014). Angiotensin
654 II mediates angiotensin converting enzyme type 2 internalization and degradation through
655 an angiotensin II type I receptor-dependent mechanism. *Hypertension, 64*(6), 1368-1375.
656 doi:10.1161/HYPERTENSIONAHA.114.03743
657 Diao, B., Wang, C., Wang, R., Feng, Z., Zhang, J., Yang, H., Tan, Y., Wang, H., Wang, C., Liu,
658 L., Liu, Y., Liu, Y., Wang, G., Yuan, Z., Hou, X., Ren, L., Wu, Y., and Chen, Y. (2021).
659 Human kidney is a target for novel severe acute respiratory syndrome coronavirus 2
660 infection. *Nat Commun, 12*(1), 2506. doi:10.1038/s41467-021-22781-1
661 Durbin, J. E., Hackenmiller, R., Simon, M. C., and Levy, D. E. (1996). Targeted disruption of the
662 mouse Stat1 gene results in compromised innate immunity to viral disease. *Cell, 84*(3),
663 443-450. doi:10.1016/s0092-8674(00)81289-1
664 Faradji, A., Bohbot, A., Schmitt-Goguel, M., Siffert, J. C., Dumont, S., Wiesel, M. L., Piemont,
665 Y., Eischen, A., Bergerat, J. P., Bartholeyns, J., and et al. (1994). Large scale isolation of
666 human blood monocytes by continuous flow centrifugation leukapheresis and counterflow
667 centrifugation elutriation for adoptive cellular immunotherapy in cancer patients. *J*
668 *Immunol Methods, 174*(1-2), 297-309. doi:10.1016/0022-1759(94)90033-7
669 Feng, Z., Diao, B., Wang, R., Wang, G., Wang, C., Tan, Y., Liu, L., Wang, C., Liu, Y., Liu, Y.,
670 Yuan, Z., Ren, L., Wu, Y., and Chen, Y. (2020). The novel severe acute respiratory
671 syndrome coronavirus 2 (SARS-CoV-2) directly decimates human spleens and lymph
672 nodes. *medRxiv*, 2020.2003.2027.20045427. doi:10.1101/2020.03.27.20045427
673 Ferrario, C. M., Jessup, J., Chappell, M. C., Averill, D. B., Brosnihan, K. B., Tallant, E. A., Diz,
674 D. I., and Gallagher, P. E. (2005). Effect of angiotensin-converting enzyme inhibition and
675 angiotensin II receptor blockers on cardiac angiotensin-converting enzyme 2. *Circulation,*
676 *111*(20), 2605-2610. doi:10.1161/CIRCULATIONAHA.104.510461
677 Field, A. K., Tytell, A. A., Lampson, G. P., and Hilleman, M. R. (1967). Inducers of interferon
678 and host resistance. II. Multistranded synthetic polynucleotide complexes. *Proc Natl Acad*
679 *Sci U S A, 58*(3), 1004-1010. doi:10.1073/pnas.58.3.1004

680 Gao, L., Kumar, V., Vellichirammal, N. N., Park, S. Y., Rudebush, T. L., Yu, L., Son, W. M.,
681 Pekas, E. J., Wafi, A. M., Hong, J., Xiao, P., Guda, C., Wang, H. J., Schultz, H. D., and
682 Zucker, I. H. (2020). Functional, proteomic and bioinformatic analyses of Nrf2- and
683 Keap1- null skeletal muscle. *J Physiol, 598*(23), 5427-5451. doi:10.1113/JP280176
684 Gavriatopoulou, M., Korompoki, E., Fotiou, D., Ntanasis-Stathopoulos, I., Psaltopoulou, T.,
685 Kastritis, E., Terpos, E., and Dimopoulos, M. A. (2020). Organ-specific manifestations of
686 COVID-19 infection. *Clin Exp Med, 20*(4), 493-506. doi:10.1007/s10238-020-00648-x
687 Gendelman, H. E., Baca, L. M., Kubrak, C. A., Genis, P., Burrous, S., Friedman, R. M., Jacobs,
688 D., and Meltzer, M. S. (1992). Induction of IFN-alpha in peripheral blood mononuclear
689 cells by HIV-infected monocytes. Restricted antiviral activity of the HIV-induced IFN. *J*
690 *Immunol, 148*(2), 422-429. Retrieved from
691 https://www.ncbi.nlm.nih.gov/pubmed/1729362
692 Guan, W. J., Ni, Z. Y., Hu, Y., Liang, W. H., Ou, C. Q., He, J. X., Liu, L., Shan, H., Lei, C. L.,
693 Hui, D. S. C., Du, B., Li, L. J., Zeng, G., Yuen, K. Y., Chen, R. C., Tang, C. L., Wang, T.,
694 Chen, P. Y., Xiang, J., Li, S. Y., Wang, J. L., Liang, Z. J., Peng, Y. X., Wei, L., Liu, Y.,
695 Hu, Y. H., Peng, P., Wang, J. M., Liu, J. Y., Chen, Z., Li, G., Zheng, Z. J., Qiu, S. Q., Luo,
696 J., Ye, C. J., Zhu, S. Y., Zhong, N. S., and China Medical Treatment Expert Group for, C.
697 (2020). Clinical characteristics of coronavirus disease 2019 in China. *N Engl J Med,*
698 *382*(18), 1708-1720. doi:10.1056/NEJMoa2002032
699 Hayden, M. S., and Ghosh, S. (2004). Signaling to NF-kappaB. *Genes Dev, 18*(18), 2195-2224.
700 doi:10.1101/gad.1228704
701 Her, Z., Malleret, B., Chan, M., Ong, E. K., Wong, S. C., Kwek, D. J., Tolou, H., Lin, R. T.,
702 Tambyah, P. A., Renia, L., and Ng, L. F. (2010). Active infection of human blood
703 monocytes by Chikungunya virus triggers an innate immune response. *J Immunol, 184*(10),
704 5903-5913. doi:10.4049/jimmunol.0904181
705 Huang, C., Wang, Y., Li, X., Ren, L., Zhao, J., Hu, Y., Zhang, L., Fan, G., Xu, J., Gu, X., Cheng,
706 Z., Yu, T., Xia, J., Wei, Y., Wu, W., Xie, X., Yin, W., Li, H., Liu, M., Xiao, Y., Gao, H.,
707 Guo, L., Xie, J., Wang, G., Jiang, R., Gao, Z., Jin, Q., Wang, J., and Cao, B. (2020). Clinical
708 features of patients infected with 2019 novel coronavirus in Wuhan, China. *Lancet,*
709 *395*(10223), 497-506. doi:10.1016/S0140-6736(20)30183-5

710 Huang da, W., Sherman, B. T., and Lempicki, R. A. (2009). Systematic and integrative analysis
711 of large gene lists using DAVID bioinformatics resources. *Nat Protoc, 4*(1), 44-57.
712 doi:10.1038/nprot.2008.211
713 Krzyzowska, M., Baska, P., Orlowski, P., Zdanowski, R., Winnicka, A., Eriksson, K., and
714 Stankiewicz, W. (2013). HSV-2 regulates monocyte inflammatory response via the
715 Fas/FasL pathway. *PLoS One, 8*(7), e70308. doi:10.1371/journal.pone.0070308
716 Kuwabara, T., Ishikawa, F., Kondo, M., and Kakiuchi, T. (2017). The role of IL-17 and related
717 cytokines in inflammatory autoimmune diseases. *Mediators Inflamm, 2017*, 3908061.
718 doi:10.1155/2017/3908061
719 Lambert, D. W., Yarski, M., Warner, F. J., Thornhill, P., Parkin, E. T., Smith, A. I., Hooper, N.
720 M., and Turner, A. J. (2005). Tumor necrosis factor-alpha convertase (ADAM17) mediates
721 regulated ectodomain shedding of the severe-acute respiratory syndrome-coronavirus
722 (SARS-CoV) receptor, angiotensin-converting enzyme-2 (ACE2). *J Biol Chem, 280*(34),
723 30113-30119. doi:10.1074/jbc.M505111200
724 Li, F. (2016). Structure, Function, and Evolution of Coronavirus Spike Proteins. *Annu Rev Virol,*
725 *3*(1), 237-261. doi:10.1146/annurev-virology-110615-042301
726 Liao, M., Liu, Y., Yuan, J., Wen, Y., Xu, G., Zhao, J., Cheng, L., Li, J., Wang, X., Wang, F., Liu,
727 L., Amit, I., Zhang, S., and Zhang, Z. (2020). Single-cell landscape of bronchoalveolar
728 immune cells in patients with COVID-19. *Nat Med, 26*(6), 842-844. doi:10.1038/s41591-
729 020-0901-9
730 Liu, X., Jana, M., Dasgupta, S., Koka, S., He, J., Wood, C., and Pahan, K. (2002). Human
731 immunodeficiency virus type 1 (HIV-1) tat induces nitric-oxide synthase in human
732 astroglia. *J Biol Chem, 277*(42), 39312-39319. doi:10.1074/jbc.M205107200
733 Lu, L., Zhang, H., Dauphars, D. J., and He, Y. W. (2021). A potential role of interleukin 10 in
734 COVID-19 pathogenesis. *Trends Immunol, 42*(1), 3-5. doi:10.1016/j.it.2020.10.012
735 Lu, R., Zhao, X., Li, J., Niu, P., Yang, B., Wu, H., Wang, W., Song, H., Huang, B., Zhu, N., Bi,
736 Y., Ma, X., Zhan, F., Wang, L., Hu, T., Zhou, H., Hu, Z., Zhou, W., Zhao, L., Chen, J.,
737 Meng, Y., Wang, J., Lin, Y., Yuan, J., Xie, Z., Ma, J., Liu, W. J., Wang, D., Xu, W.,
738 Holmes, E. C., Gao, G. F., Wu, G., Chen, W., Shi, W., and Tan, W. (2020). Genomic
739 characterisation and epidemiology of 2019 novel coronavirus: implications for virus

740 origins and receptor binding. *Lancet, 395*(10224), 565-574. doi:10.1016/S0140-
741 6736(20)30251-8
742 Lugo-Villarino, G., Cougoule, C., Meunier, E., Rombouts, Y., Verollet, C., and Balboa, L. (2019).
743 Editorial: The mononuclear phagocyte system in infectious disease. *Front Immunol, 10*,
744 1443. doi:10.3389/fimmu.2019.01443
745 Lum, F. M., Lee, D., Chua, T. K., Tan, J. J. L., Lee, C. Y. P., Liu, X., Fang, Y., Lee, B., Yee, W.
746 X., Rickett, N. Y., Chia, P. Y., Lim, V., Leo, Y. S., Matthews, D. A., Hiscox, J. A., and
747 Ng, L. F. P. (2018). Zika virus infection preferentially counterbalances human peripheral
748 monocyte and/or NK cell activity. *mSphere, 3*(2). doi:10.1128/mSphereDirect.00120-18
749 Mendoza, E. J., Manguiat, K., Wood, H., and Drebot, M. (2020). Two detailed plaque assay
750 protocols for the quantification of infectious SARS-CoV-2. *Curr Protoc Microbiol, 57*(1),
751 ecpmc105. doi:10.1002/cpmc.105
752 Merad, M., and Martin, J. C. (2020). Pathological inflammation in patients with COVID-19: a key
753 role for monocytes and macrophages. *Nat Rev Immunol, 20*(6), 355-362.
754 doi:10.1038/s41577-020-0331-4
755 Mukadam, I. Z., Machhi, J., Herskovitz, J., Hasan, M., Oleynikov, M. D., Blomberg, W. R.,
756 Svechkarev, D., Mohs, A. M., Zhou, Y., Dash, P., McMillan, J., Gorantla, S., Garrison, J.,
757 Gendelman, H. E., and Kevadiya, B. D. (2020). Rilpivirine-associated aggregation-induced
758 emission enables cell-based nanoparticle tracking. *Biomaterials, 231*, 119669.
759 doi:10.1016/j.biomaterials.2019.119669
760 Nikitina, E., Larionova, I., Choinzonov, E., and Kzhyshkowska, J. (2018). Monocytes and
761 macrophages as viral targets and reservoirs. *Int J Mol Sci, 19*(9).
762 doi:10.3390/ijms19092821
763 Pedrosa, M. A., Valenzuela, R., Garrido-Gil, P., Labandeira, C. M., Navarro, G., Franco, R.,
764 Labandeira-Garcia, J. L., and Rodriguez-Perez, A. I. (2021). Experimental data using
765 candesartan and captopril indicate no double-edged sword effect in COVID-19. *Clin Sci*
766 *(Lond), 135*(3), 465-481. doi:10.1042/CS20201511
767 Perlman, S., and Netland, J. (2009). Coronaviruses post-SARS: update on replication and
768 pathogenesis. *Nat Rev Microbiol, 7*(6), 439-450. doi:10.1038/nrmicro2147

769 Pichlmair, A., Schulz, O., Tan, C. P., Naslund, T. I., Liljestrom, P., Weber, F., and Reis e Sousa,
770 C. (2006). RIG-I-mediated antiviral responses to single-stranded RNA bearing 5'-
771 phosphates. *Science, 314*(5801), 997-1001. doi:10.1126/science.1132998
772 Ruan, Q., Yang, K., Wang, W., Jiang, L., and Song, J. (2020). Clinical predictors of mortality due
773 to COVID-19 based on an analysis of data of 150 patients from Wuhan, China. *Intensive*
774 *Care Med, 46*(5), 846-848. doi:10.1007/s00134-020-05991-x
775 Rubinstein, S., Familletti, P. C., and Pestka, S. (1981). Convenient assay for interferons. *J Virol,*
776 *37*(2), 755-758. doi:10.1128/JVI.37.2.755-758.1981
777 Salamanna, F., Maglio, M., Landini, M. P., and Fini, M. (2020). Body Localization of ACE-2: On
778 the Trail of the Keyhole of SARS-CoV-2. *Front Med (Lausanne), 7*, 594495.
779 doi:10.3389/fmed.2020.594495
780 Schmidtmayerova, H., Nottet, H. S., Nuovo, G., Raabe, T., Flanagan, C. R., Dubrovsky, L.,
781 Gendelman, H. E., Cerami, A., Bukrinsky, M., and Sherry, B. (1996). Human
782 immunodeficiency virus type 1 infection alters chemokine beta peptide expression in
783 human monocytes: implications for recruitment of leukocytes into brain and lymph nodes.
784 *Proc Natl Acad Sci U S A, 93*(2), 700-704. doi:10.1073/pnas.93.2.700
785 Shang, J., Wan, Y., Luo, C., Ye, G., Geng, Q., Auerbach, A., and Li, F. (2020). Cell entry
786 mechanisms of SARS-CoV-2. *Proc Natl Acad Sci U S A, 117*(21), 11727-11734.
787 doi:10.1073/pnas.2003138117
788 Soler, M. J., Ye, M., Wysocki, J., William, J., Lloveras, J., and Batlle, D. (2009). Localization of
789 ACE2 in the renal vasculature: amplification by angiotensin II type 1 receptor blockade
790 using telmisartan. *Am J Physiol Renal Physiol, 296*(2), F398-405.
791 doi:10.1152/ajprenal.90488.2008
792 Swiecki, M., and Colonna, M. (2011). Type I interferons: diversity of sources, production
793 pathways and effects on immune responses. *Curr Opin Virol, 1*(6), 463-475.
794 doi:10.1016/j.coviro.2011.10.026
795 Szklarczyk, D., Gable, A. L., Lyon, D., Junge, A., Wyder, S., Huerta-Cepas, J., Simonovic, M.,
796 Doncheva, N. T., Morris, J. H., Bork, P., Jensen, L. J., and Mering, C. V. (2019). STRING
797 v11: protein-protein association networks with increased coverage, supporting functional
798 discovery in genome-wide experimental datasets. *Nucleic Acids Res, 47*(D1), D607-D613.
799 doi:10.1093/nar/gky1131

800 Wan, Y., Shang, J., Graham, R., Baric, R. S., and Li, F. (2020). Receptor recognition by the novel
801 coronavirus from Wuhan: An analysis based on decade-long structural studies of SARS
802 coronavirus. *J Virol, 94*(7). doi:10.1128/JVI.00127-20
803 World Health Organization. (2020). Coronavirus disease 2019 (COVID-19). Situation report – 51.
804 Retrieved from https://www.who.int/docs/default-source/coronaviruse/situation-
805 reports/20200311-sitrep-51-covid-19.pdf?sfvrsn=1ba62e57_10
806 Wu, G., Dawson, E., Duong, A., Haw, R., and Stein, L. (2014). ReactomeFIViz: a Cytoscape app
807 for pathway and network-based data analysis. *F1000Res, 3*, 146.
808 doi:10.12688/f1000research.4431.2
809 Xia, H., Cao, Z., Xie, X., Zhang, X., Chen, J. Y., Wang, H., Menachery, V. D., Rajsbaum, R., and
810 Shi, P. Y. (2020). Evasion of type I interferon by SARS-CoV-2. *Cell Rep, 33*(1), 108234.
811 doi:10.1016/j.celrep.2020.108234
812 Xiong, Y., Liu, Y., Cao, L., Wang, D., Guo, M., Jiang, A., Guo, D., Hu, W., Yang, J., Tang, Z.,
813 Wu, H., Lin, Y., Zhang, M., Zhang, Q., Shi, M., Liu, Y., Zhou, Y., Lan, K., and Chen, Y.
814 (2020). Transcriptomic characteristics of bronchoalveolar lavage fluid and peripheral
815 blood mononuclear cells in COVID-19 patients. *Emerg Microbes Infect, 9*(1), 761-770.
816 doi:10.1080/22221751.2020.1747363
817 Xu, Z., Shi, L., Wang, Y., Zhang, J., Huang, L., Zhang, C., Liu, S., Zhao, P., Liu, H., Zhu, L., Tai,
818 Y., Bai, C., Gao, T., Song, J., Xia, P., Dong, J., Zhao, J., and Wang, F. S. (2020).
819 Pathological findings of COVID-19 associated with acute respiratory distress syndrome.
820 *Lancet Respir Med, 8*(4), 420-422. doi:10.1016/S2213-2600(20)30076-X
821 Yang, D., Chu, H., Hou, Y., Chai, Y., Shuai, H., Lee, A. C., Zhang, X., Wang, Y., Hu, B., Huang,
822 X., Yuen, T. T., Cai, J. P., Zhou, J., Yuan, S., Zhang, A. J., Chan, J. F., and Yuen, K. Y.
823 (2020). Attenuated interferon and proinflammatory response in SARS-CoV-2-infected
824 human dendritic cells is associated with viral antagonism of STAT1 phosphorylation. *J*
825 *Infect Dis, 222*(5), 734-745. doi:10.1093/infdis/jiaa356
826 Yilla, M., Harcourt, B. H., Hickman, C. J., McGrew, M., Tamin, A., Goldsmith, C. S., Bellini, W.
827 J., and Anderson, L. J. (2005). SARS-coronavirus replication in human peripheral
828 monocytes/macrophages. *Virus Res, 107*(1), 93-101. doi:10.1016/j.virusres.2004.09.004
829 Zheng, J., Wang, Y., Li, K., Meyerholz, D. K., Allamargot, C., and Perlman, S. (2021). Severe
830 acute respiratory syndrome coronavirus 2-induced immune activation and death of

831 monocyte-derived human macrophages and dendritic cells. *J Infect Dis, 223*(5), 785-795.
832 doi:10.1093/infdis/jiaa753
833 Zhou, J., Chu, H., Li, C., Wong, B. H., Cheng, Z. S., Poon, V. K., Sun, T., Lau, C. C., Wong, K.
834 K., Chan, J. Y., Chan, J. F., To, K. K., Chan, K. H., Zheng, B. J., and Yuen, K. Y. (2014).
835 Active replication of Middle East respiratory syndrome coronavirus and aberrant induction
836 of inflammatory cytokines and chemokines in human macrophages: implications for
837 pathogenesis. *J Infect Dis, 209*(9), 1331-1342. doi:10.1093/infdis/jit504
838

Supplementary information

Defining the Immune Responses for SARS-CoV-2-Human Macrophage Interactions

Mai M. Abdelmoaty[1,2], Pravin Yeapuri[1], Jatin Machhi[3], Katherine E. Olson[3], Farah Shahjin[3], You Zhou[4], Liang Jingjing[3], Kabita Pandey[3], Arpan Acharya[3], Siddappa N. Byrareddy[3], R. Lee Mosley[3] and Howard E. Gendelman[3*]

[1]Department of Pharmaceutical Sciences, College of Pharmacy, University of Nebraska Medical Center, NE 68198, USA

[2]Therapeutic Chemistry Department, Pharmaceutical and Drug Industries Research Division, National Research Centre, Giza, Egypt

[3]Department of Pharmacology and Experimental Neuroscience, College of Medicine, University of Nebraska Medical Center, NE 68198, USA

[4]Center for Biotechnology, University of Nebraska-Lincoln, Lincoln, NE, USA

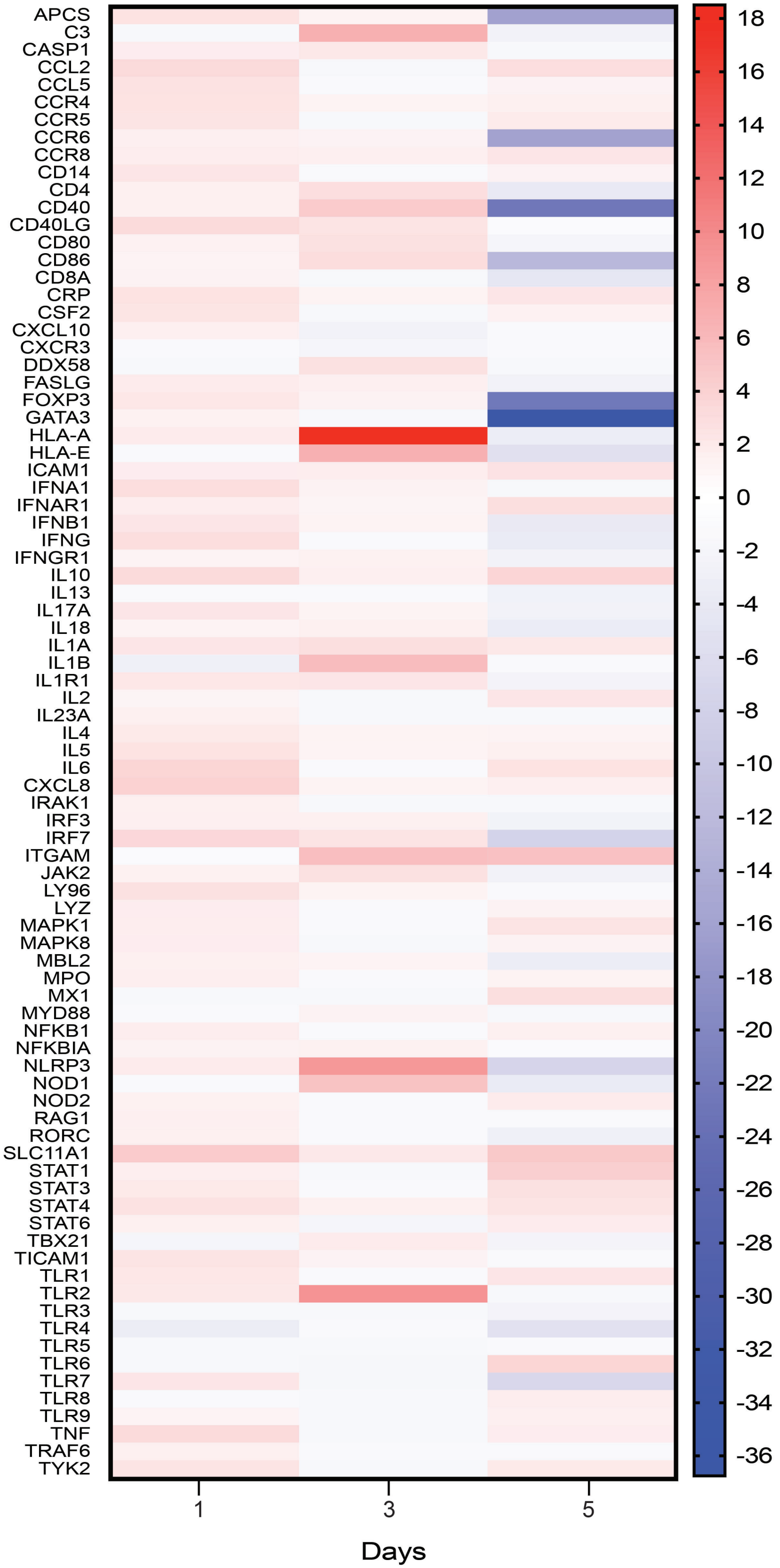
APCS
C3
CASP1
CCL2
CCL5
CCR4
CCR5
CCR6
CCR8
CD14
CD4
CD40
CD40LG
CD80
CD86
CD8A
CRP
CSF2
CXCL10
CXCR3
DDX58
FASLG
FOXP3
GATA3
HLA-A
HLA-E
ICAM1
IFNA1
IFNAR1
IFNB1
IFNG
IFNGR1
IL10
IL13
IL17A
IL18
IL1A
IL1B
IL1R1
IL2
IL23A
IL4
IL5
IL6
CXCL8
IRAK1
IRF3
IRF7
ITGAM
JAK2
LY96
LYZ
MAPK1
MAPK8
MBL2
MPO
MX1
MYD88
NFKB1
NFKBIA
NLRP3
NOD1
NOD2
RAG1
RORC
SLC11A1
STAT1
STAT3
STAT4
STAT6
TBX21
TICAM1
TLR1
TLR2
TLR3
TLR4
TLR5
TLR6
TLR7
TLR8
TLR9
TNF
TRAF6
TYK2
1
3
5
Days
18
16
14
12
10
8
6
4
2
0
-2
-4
-6
-8
-10
-12
-14
-16
-18
-20
-22
-24
-26
-28
-30
-32
-34
-36

Supplementary Figure 1. Fold changes of immune response genes in SARS-CoV-2-challenged MDMs. Heat map of fold changes in the expression of 84 genes specific for human innate and adaptive immune responses in SARS-CoV-2-challenged MDMs compared to mock-challenged MDMs at different time points after the infection, determined using RT2 Profiler Human Innate and Adaptive Immune Response 96-well Array. Fold changes were determined via Qiagen's RT2 Profiler analysis software (n=4).

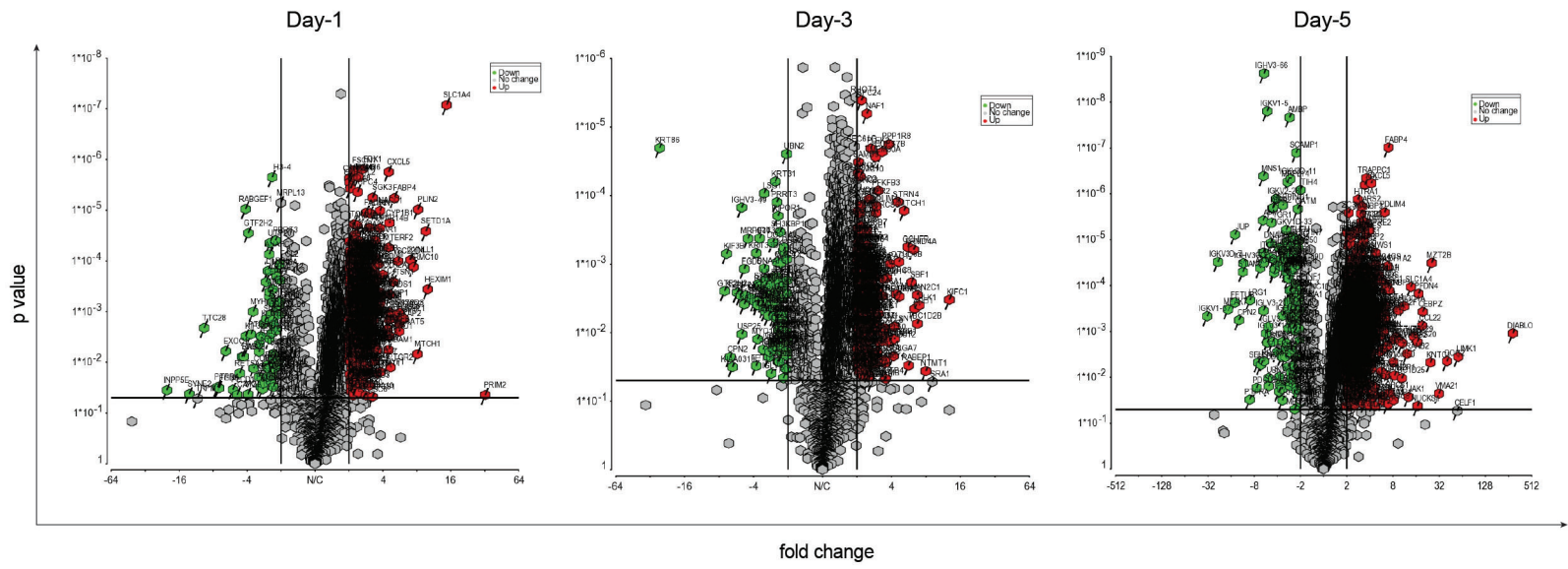

Day-1
Day-3
Day-5
p value
fold change
Down
No change
Up

Supplementary Figure 2. Differential proteomic analysis of SARS-CoV-2-challenged MDMs. Volcano plots showing the fold change plotted against the P value highlighting significantly changed proteins (red – upregulation and green – downregulation; $p \leq 0.05$ and an absolute fold change ≥ 2) in SARS-CoV-2-challenged MDMs compared to mock-challenged MDMs at different time points (n=4). The vertical lines correspond to the absolute fold change of 2, and the horizontal line represents a p value of 0.05.